European Journal of Medicinal Chemistry 129 (2017) 287–302

Contents lists available at ScienceDirect

European Journal of Medicinal Chemistry

journal homepage: http://www.elsevier.com/locate/ejmech

Research paper

Design, synthesis, biological evaluation and X-ray structural studies of potent human dihydroorotate dehydrogenase inhibitors based on hydroxylated azole scaffolds

Stefano Sainas [a, 1], Agnese C. Pippione [a, 1], Marta Giorgis [a], Elisa Lupino [b], Parveen Goyal [c], Cristina Ramondetti [b], Barbara Buccinnà [b], Marco Piccinini [b], Rodolpho C. Braga [d], Carolina H. Andrade [d], Mikael Andersson [c], Ann-Christin Moritzer [c, e], Rosmarie Friemann [c, f], Stefano Mensa [g], Salam Al-Kadaraghi [h], Donatella Boschi [a], Marco L. Lolli [a, *]

[a] Department of Science and Drug Technology, University of Torino, via Pietro Giuria 9, 10125 Torino, Italy
[b] Department of Oncology, University of Torino, via Michelangelo 27/B, 10126 Torino, Italy
[c] Department of Chemistry and Molecular Biology, University of Gothenburg, Box 462, S-40530 Gothenburg Sweden
[d] LabMol, Faculty of Pharmacy, Federal University of Goias, 74605-170 Goiania, Brazil
[e] Department of Chemistry, Biochemistry, University of Bielefeld, Universitätsstraße 25, 33615 Bielefeld, Germany
[f] Department of Structural Biology, Stanford University School of Medicine, 299 Campus Drive West Stanford, CA 94305-5126, USA
[g] Stephenson Institute for Renewable Energy, Department of Chemistry, University of Liverpool, L69 7ZF Liverpool, UK
[h] Department of Biochemistry and Structural Biology, Lund University, Sweden

ARTICLE INFO

Article history:
Received 25 November 2016
Received in revised form
6 February 2017
Accepted 7 February 2017
Available online 14 February 2017

Keywords:
Dihydroorotate dehydrogenase (DHODH) inhibitors
X-ray-crystallography
Autoimmune diseases
Leflunomide
Brequinar
Bioisosterism

ABSTRACT

A new generation of potent *h*DHODH inhibitors designed by a scaffold-hopping replacement of the quinolinecarboxylate moiety of brequinar, one of the most potent known *h*DHODH inhibitors, is presented here. Their general structure is characterized by a biphenyl moiety joined through an amide bridge with an acidic hydroxyazole scaffold (hydroxylated thiadiazole, pyrazole and triazole). Molecular modelling suggested that these structures should adopt a brequinar-like binding mode involving interactions with subsites 1, 2 and 4 of the *h*DHODH binding site. Initially, the inhibitory activity of the compounds was studied on recombinant *h*DHODH. The most potent compound of the series in the enzymatic assays was the thiadiazole analogue **4** (IC_{50} 16 nM). The activity was found to be dependent on the fluoro substitution pattern at the biphenyl moiety as well as on the choice/substitution of the heterocyclic ring. Structure determination of *h*DHODH co-crystallized with one representative compound from each series (**4**, **5** and **6**) confirmed the brequinar-like binding mode as suggested by modelling. The specificity of the observed effects of the compound series was tested in cell-based assays for antiproliferation activity using Jurkat cells and PHA-stimulated PBMC. These tests were also verified by addition of exogenous uridine to the culture medium. In particular, the triazole analogue **6** (IC_{50} against *h*DHODH: 45 nM) exerted potent *in vitro* antiproliferative and immunosuppressive activity without affecting cell survival.

1. Introduction

Human dihydroorotate dehydrogenase (*h*DHODH), a flavin-dependent mitochondrial enzyme involved in *de novo* pyrimidine biosynthesis, is a validated therapeutic target for the treatment of autoimmune diseases such as rheumatoid arthritis and cancer [1–3]. Leflunomide (Fig. 1) is a disease-modifying anti-rheumatic drug that was approved more than 15 years ago for the treatment of

Abbreviations used: human dihydroorotate dehydrogenase, (*h*DHODH); L-dihydroorotate, (DHO); orotate, (ORO); reduced flavin mononucleotide, ($FMNH_2$); Quantum mechanics/molecular mechanics, (QM/MM); QM-Polarized Ligand Docking, (QPLD); Palladium on carbon, (Pd/C); phytohaemagglutinin, (PHA); peripheral blood mononuclear cell, (PBMC); isopropyl β-D-1-thiogalactopyranosidel, (IPTG); n-Undecyl-*N*,*N*-Dimethylamine-*N*-Oxide, (UDAO); potassium thiocyanate, (KSCN); poly-γ-glutamic acid low molecular weight, (PGA-LM).

* Corresponding author.
E-mail address: marco.lolli@unito.it (M.L. Lolli).

[1] Both authors contributed equally to this work.

http://dx.doi.org/10.1016/j.ejmech.2017.02.017
0223-5234/

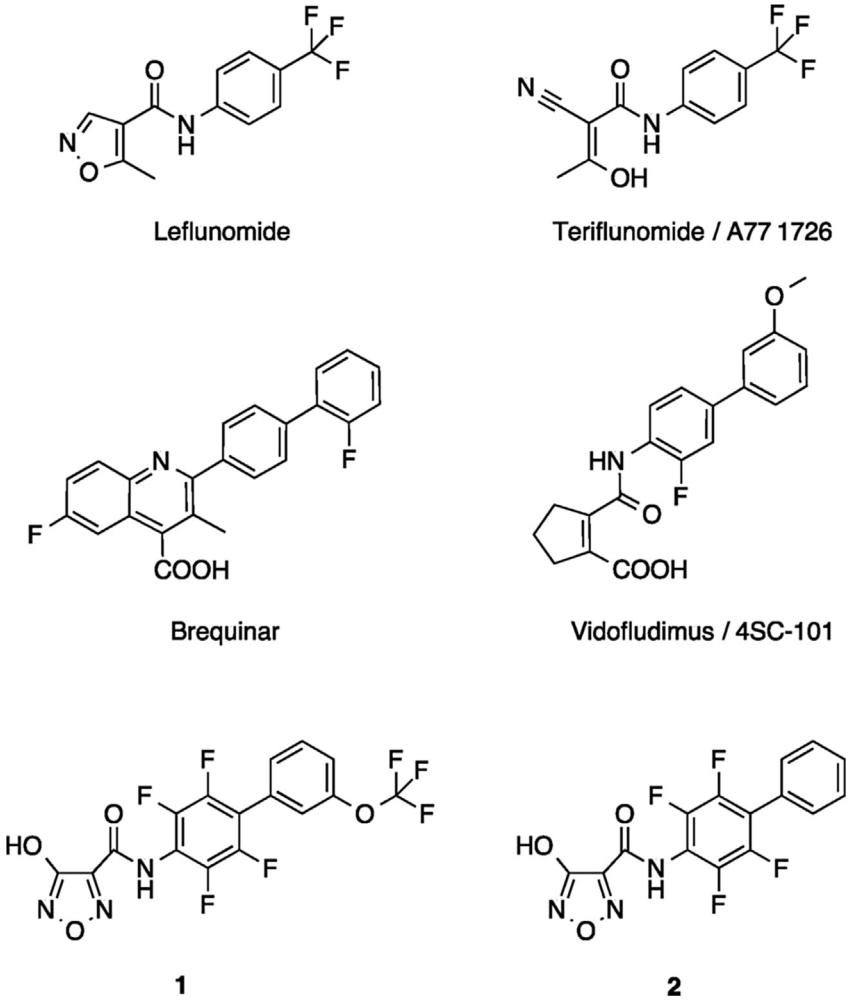

Fig. 1. Presentation of scaffolds of leflunomide, its active metabolite teriflunomide (A77 1726), brequinar, vidofludimus (4SC-101) and the hydroxyfurazan analogues **1** [5] and **2** [5].

rheumatoid arthritis and other autoimmune diseases [4].

Although associated with severe side effects such as diarrhea, abnormal liver tests, nausea, and hair loss [6], leflunomide acts as a prodrug and is rapidly converted into its active metabolite teriflunomide (also called A77 1726, Fig. 1), which is able to inhibit *h*DHODH in the low μM range [7,8]. Since the introduction of leflunomide, the search for new potent *h*DHODH inhibitors that would display similar clinical benefits as leflunomide but without associated side effects, has been on going. One of the promising compounds was brequinar [9], which was discarded as a therapeutic agent due to a narrow therapeutic window and inconsistent pharmacokinetics [2]. Another compound, 4SC-101 (vidofludimus, Fig. 1) [10], is currently undergoing phase II clinical trials for inflammatory bowel disease [6,11]. However, despite recent efforts [1,6,12–15], the quest to add new *h*DHODH inhibitors to the human pharmacopoeia remains an urgent area of research.

Earlier, we reported a series of innovative *h*DHODH inhibitors [5] designed by merging some structural features of leflunomide and brequinar and based on the acidic 4-hydroxy-1,2,5-oxadiazol-3-yl (hydroxyfurazan) moiety (Fig. 1, compounds **1** and **2**). The acidic hydroxyfurazan, connected through an amide bridge to a substituted biphenyl lipophilic moiety, was suggested to play the role of brequinar's carboxylic group by interacting with Arg136 in the *h*DHODH subsite 2 [16]. Compounds **1** and **2** were able to potently inhibit DHODH on murine liver mitochondrial membranes (50 and 66 nM respectively) [5]. The degree of fluorine substitution at the phenyl ring adjacent to the oxadiazole moiety was strongly correlated with activity. In addition, the correlation between activity and stabilization of the compounds' bioactive conformations was extensively studied [17].

Using a similar approach, in this work we describe new potent *h*DHODH inhibitors designed by selecting other acidic hydroxylated azoles, ideally substituting hydroxyfurazan in **1** and **2**. The selection of hydroxylated azole systems (specifically hydroxythiadiazole, pyrazole and triazole) was run by the possibility of establishing interactions with the small lipophilic pocket created by Val143 and Val134 (subsite 4) and by their different acidic properties [18]. Supported by promising docking scores, nine candidate structures based on three acidic heterocycles were designed and synthetized (compounds **3**–**9**, Fig. 2, Table S1).

Synthetic strategies and detailed enzymatic and cell-based studies of the designed series are presented and discussed. The suggested binding modes of the most representative molecules were confirmed by high-resolution crystal structures of *h*DHODH in complex with the compounds **4**–**6**.

2. Result and discussion

2.1. Molecular modelling

A molecular simulation of compounds **1**–**9** docked inside the *h*DHODH binding site was initially performed. Docking results,

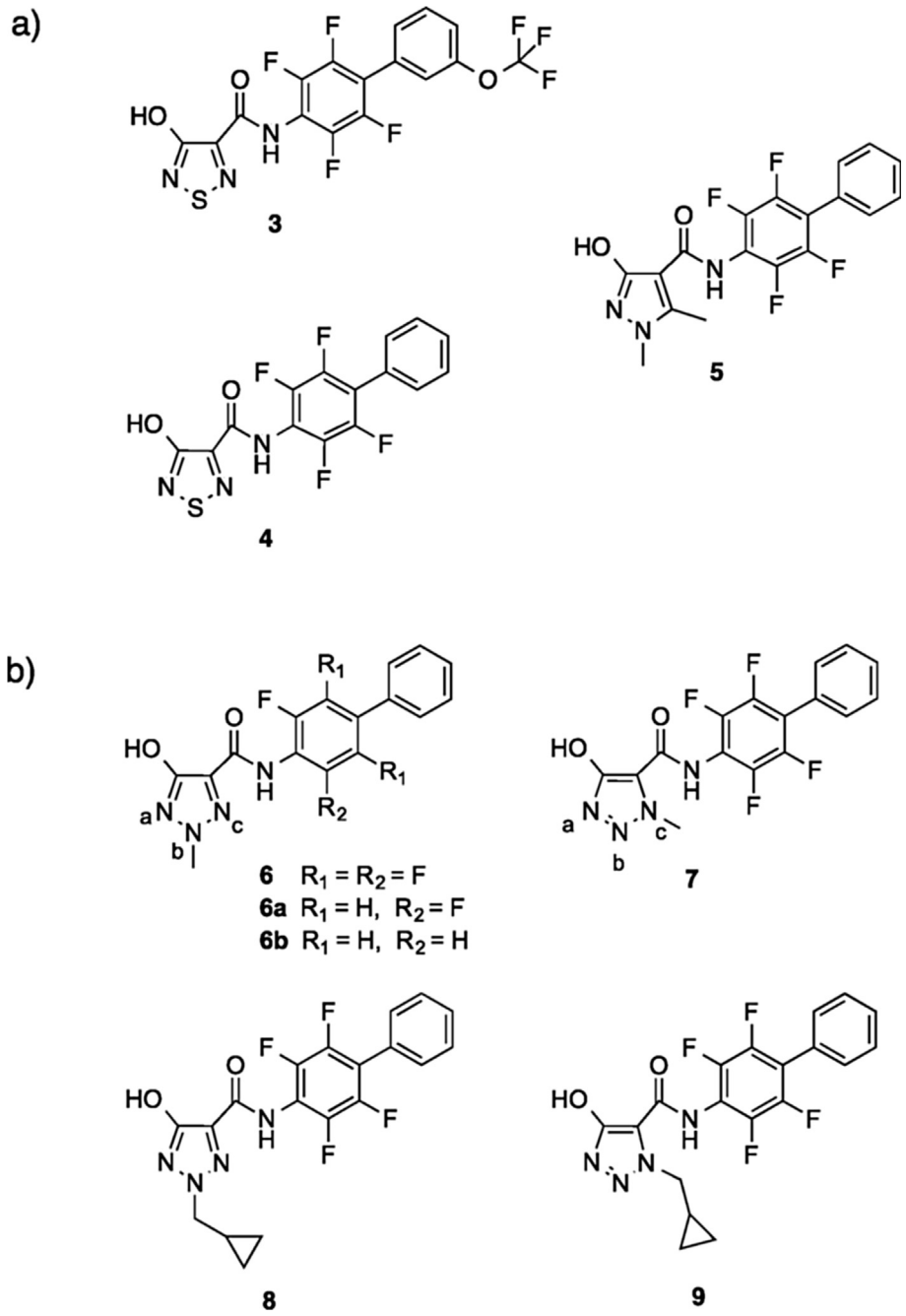

Fig. 2. (a) Structures of compounds **3**, **4** containing the hydroxythiadiazole moiety and **5** containing the hydroxypyrazole moiety. (b) Structures of compounds **6**–**9** bearing the hydroxytriazole moiety.

starting from the structure of *h*DHODH co-crystallized with a brequinar analogue (PDB id 1D3G) [19] and based on a validated protocol (root-mean-square-difference of 0.615 Å with a docking score of $\Delta G = -14.8$ kcal/mol), indicated that all designed compounds, as previously reported for analogues **1** and **2**, adopt a brequinar-like [2] binding mode. The main interactions involve the ionized hydroxyl group of the heterocyclic moiety, predicted to be oriented toward the polar subsite 2 of the binding site (Fig. 3). This moiety was observed making an ion bridge with the side chain of Arg136 and a hydrogen bond with the side chain of Gln47, thus effectively mimicking the carboxyl group of brequinar and related compounds. On the other hand, the tetrafluorinated biphenyl moiety is able to make hydrophobic contacts with the amino acids (Leu42 and Leu46) in subsite 1 (Fig. 3). In terms of docking score, the compounds range (−12.09 – −13.59, Supplementary Table 1) falls between terifluonomide (−9.21) and brequinar (−14.81) themself. Triazole **7** owed the lower score (−13.59), being just one unit higher the brequinar itself.

Besides maintaining the interactions with Arg136 and Gln47 of subsite 2, the new azole scaffolds were found able to reach the pocket of subsite 4, where Val134/Val143 are located. This small hydrophobic pocket has often been used to achieve additional ligand interactions and to increase the binding affinity. This is the case for teriflunomide, which is able to stabilize the primary subsite 4 interaction using a methyl group, and brequinar, where this role is played by a fluorine atom [19]. Leban and co-workers [20] used a

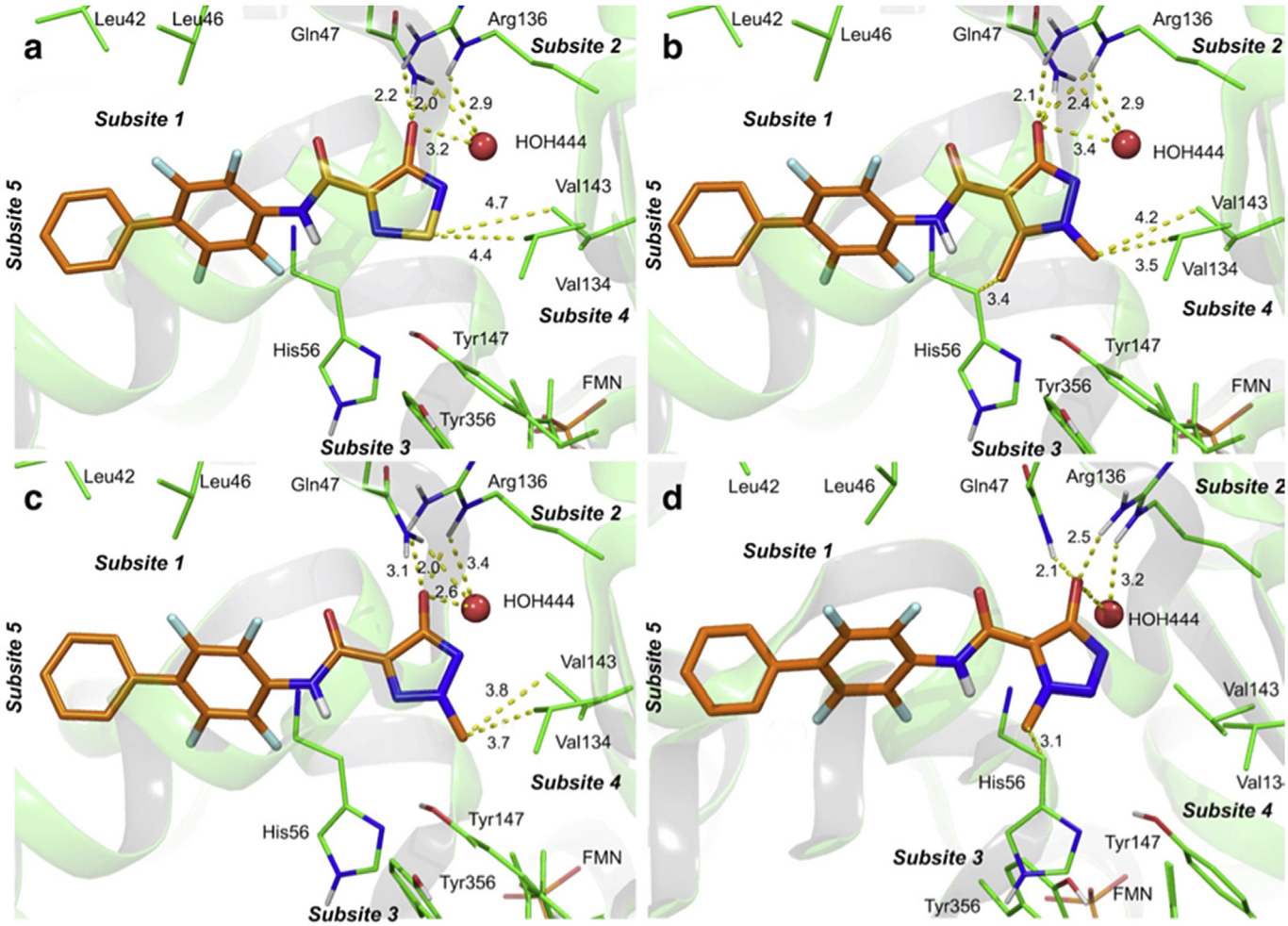

Fig. 3. Inhibitors **4**–**7** (a – d respectively) docked into the *h*DHODH ubiquinone binding site. Amino acid residues interacting with the inhibitors are shown in stick representation. A water molecule in the ubiquinone binding site is shown as a red sphere. Inhibitors **4**–**7** are presented in stick representation with carbon atoms in orange, nitrogen in blue, fluorine in cyan, oxygen in red and sulphur in yellow. The yellow dashed lines represent the hydrogen bonds and interactions involved in binding of the inhibitors, along with the distances (in Å) between the respective atoms. The figure was made using PyMOL (http://www.pymol.org) [21].

similar strategy in designing a vidofludimus analogue characterized by the presence of a thiophene sulphur atom that fits into this hydrophobic pocket. It should be noted how compounds **3**–**9** presented better docking scores then hydroxyfurazans **1**, **2** (−11.34 and −10.91, respectively), being able to establish additional interactions with the binding site of *h*DHODH. This seems indicate coherence with the strategy used for designing them.

2.2. Chemistry

The reaction scheme designed for the thiadiazole analogues **3** and **4** started from **10** [22], a hydroxythiadiazole intermediate (Scheme 1).

In order to protect the hydroxyl group in position 3, compound **10** was *O*-benzylated using benzyl bromide under basic conditions. When considering the reactivity of substituted hydroxylated azoles (such as thiadiazole itself), both *O*- and *N*- alkylation patterns must be considered. The type of the heteroatoms inside the heteroazole system, and the choice of the alkylating agent usually rule the alkylation pattern. For example, the hydroxy-1,2,5-oxadiazole system can be alkylated only on the exocyclic oxygen, while the *N*-alkylation was rarely observed [23]. Although for hydroxy-1,2,5-thiadiazole alkylation on either the exocyclic oxygen or the nitrogen in position 2 has been reported [24], the reaction with benzyl bromide of thiadiazole **10** yielded only one major reaction product (**11**, 59% yield). Compound **11** was characterized as the *O*-benzyl isomer on the basis of the ^{13}C-chemical shift of the methylene benzylic position found at δ 73.5 ppm, whereas the *N*-benzylated isomers were upshifted to around 50 ppm [25]. These data were also found to be coherent with *O*-benzylated hydroxytriazoles **23** and **24**, both characterized by heteronuclear 2D-NMR (HSQC and HMBC) experiments [26]. The nitrile **11** was then hydrolysed to the corresponding acid **12**, this latter transformed into its corresponding acyl chloride that was allowed to react with the appropriate aniline (**13** or **14**) to give the protected thiadiazole amides **15** and **16**, respectively. Application of standard catalytic hydrogenation conditions to **15** and **16** for the removal of the benzyl moiety did not gave any reaction product, probably due to the poisoning of the palladium catalyst by the thiadiazolic sulphur atom. Compounds **3** and **4** were obtained from **15** and **16** by treatment with trifluoroacetic acid under moderate heating.

The synthesis of the pyrazole analogue **5**, shown in Scheme 2, started from hydroxypyrazole **18**, readily obtained in 71% yield by treatment of diethyl 2-(1-ethoxyethylidene)propanedioate **17** with methylhydrazine in the presence of sodium ethoxide.

We verified the relative position of methyl group of compound

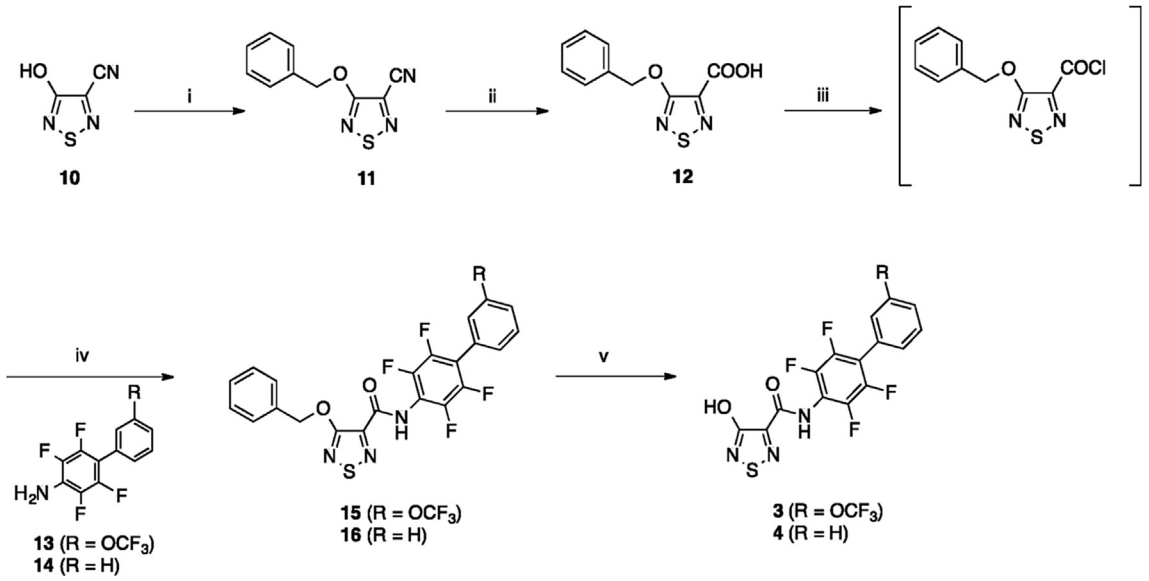

Scheme 1. Synthesis of thiadiazole analogues **3** and **4**: i) BnBr, K_2CO_3, dry DMF; ii) a) 2 M NaOH, MeOH, reflux; b) 2 M HCl; iii) oxalyl chloride, DMF, dry THF; iv) dry pyridine, dry toluene; v) TFA, 70 °C.

18, through the diagnostic ^{1}H-^{13}C HMBC correlation between the ^{1}H signal of N(1)-methyl substituent and the ^{13}C signal of C-5 of the pyrazol ring and the absence of a similar correlation between ^{1}H signal of N(1)-methyl substituent and the ^{13}C signal of C-3 of the pyrazol ring (Supplement Figs. S1 and S2). Subsequently, crystal structures of *h*DHODH in complexes with compound **5** (see Chapter 2.4) confirmed the position of methyl group in N(1) atom. The hydroxypyrazole **18** was *O*-benzylated producing **19** (the ^{13}C NMR methylene benzylic position signal at δ 70.0 ppm is consistent with what was observed in **11**). The hydrolysis of **19** produced the acid **20**, which was then converted into its corresponding acyl chloride. The latter, probably due to steric hindrance, was found to be quite unreactive towards the weakly nucleophilic aniline **14**. To resolve this problem, the aniline **14** was converted into its dimethylalluminiumamide, reactive enough to produce the desired amide **21** in 72% yield. The benzyl-protected compound **21** was then converted to **5** by applying standard catalytic hydrogenation conditions.

The synthesis of the triazole analogues **6**–**9** (Scheme 3) started from the isomeric triazole building-blocks **23**–**26**, obtained from unsubstituted triazole **22** by a methodology for preparation of regio-substituted hydroxytriazoles we recently described [18].

The hydrolysis of the esters **23**–**26** to their corresponding carboxylic acids **27**–**30** was followed by conversion into the corresponding acyl chlorides that were allowed to react with the appropriate aniline to generate the protected triazole amides **31**–**36**. These products were converted into the triazole targets **6**–**9** by applying standard catalytic hydrogenation conditions.

2.3. Inhibition of hDHODH and structure-activity relationships (SAR)

The inhibition of recombinant *h*DHODH by compounds **3**–**9** (Fig. 2) was firstly evaluated and compared with inhibition data given from the leads teriflunomide, brequinar and the two

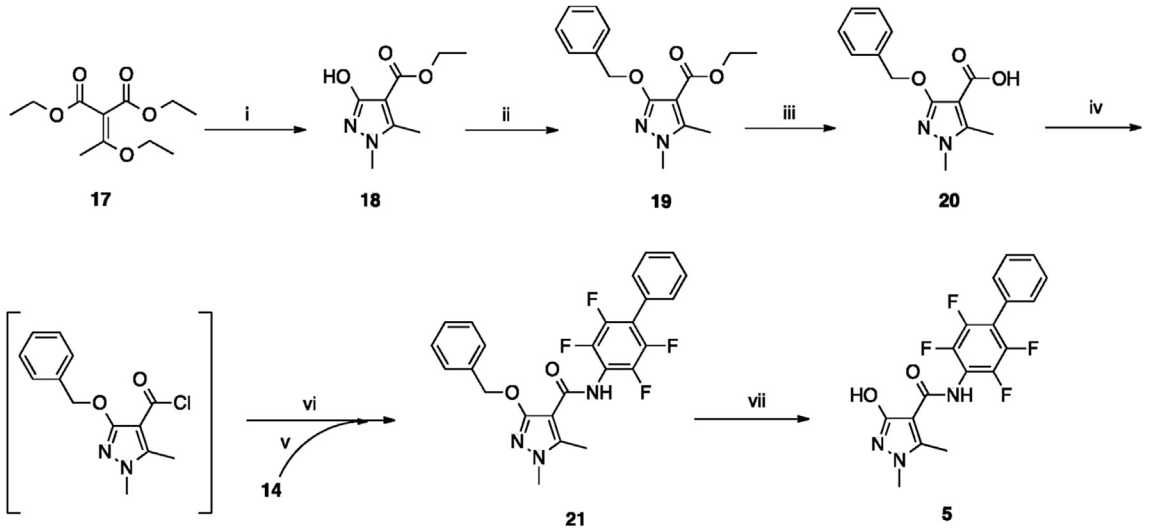

Scheme 2. Synthesis of the pyrazole analogue **5**: i) NH_2NHCH_3, sodium ethoxide, 0 °C; ii) BnBr, K_2CO_3, dry DMF; iii) a) 6 M NaOH, EtOH; b) 2 M HCl; iv) oxalyl chloride, DMF, dry THF; v) $AlMe_3$, dry toluene, rt; vi) dry toluene, reflux; vii) H_2, Pd/C, dry THF.

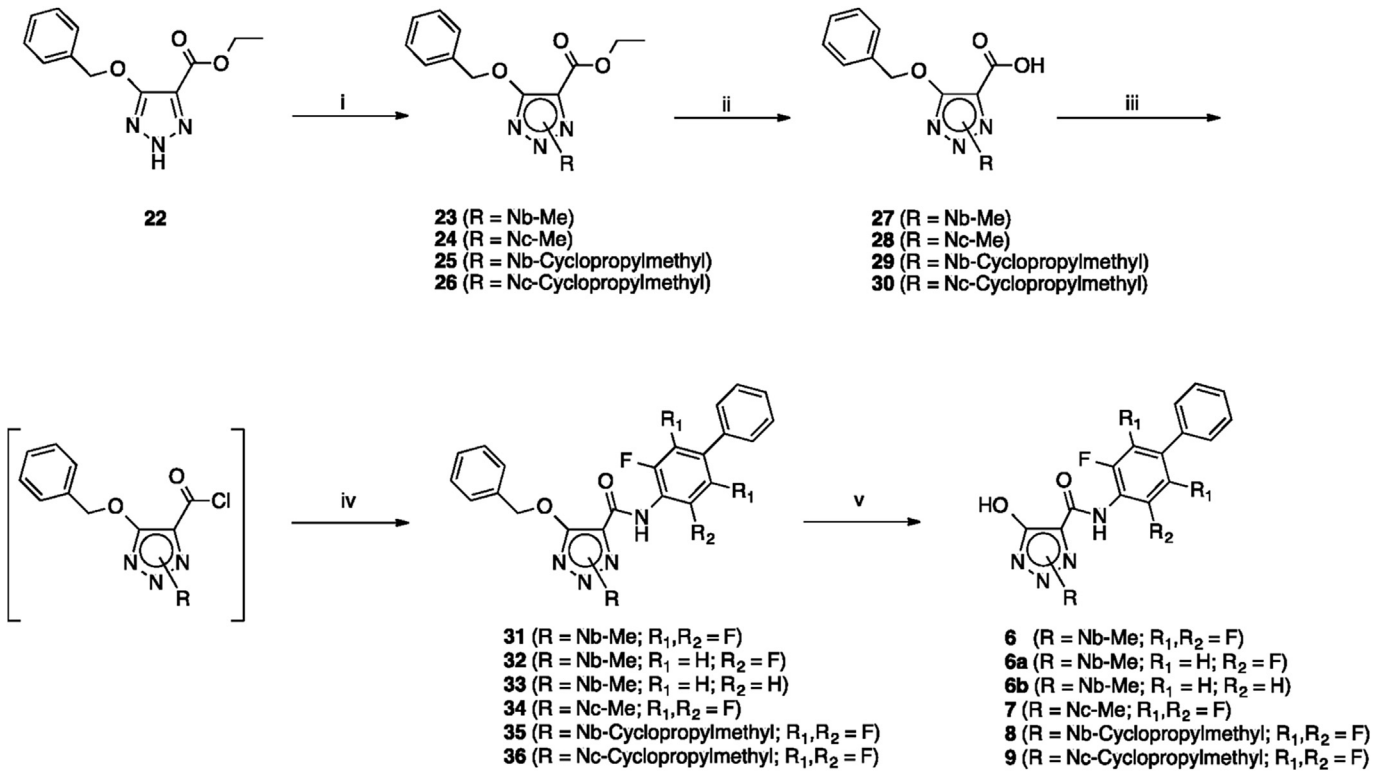

Scheme 3. Synthesis of triazole analogues **6**–**9**: i) alkyl bromide, K_2CO_3, dry acetonitrile; ii) a) 5 M NaOH, EtOH; b) 2 M HCl; iii) oxalyl chloride, DMF, dry THF; iv) fluoro-substituted biphenylamine, dry pyridine, dry toluene; v) H_2, Pd/C, dry THF.

hydroxyfurazan analogues **1** and **2** (Table 1).

Firstly, it can be observed how, moving to *h*DHODH isoform, compounds **1** and **2** were unable to repeat the potent inhibition observed on murine liver mitochondrial membranes (50 and 66 nM respectively) [5]. However, they were active as *h*DHODH inhibitors in the same range of teriflunomide. Moreover, the substitution (OCF_3 (**1**) vs H (**2**)) on the meta position of the second ring seemed to be detrimental for activity, since compound **2** that lacks this substitution is the most active. The thiadiazole analogues **3** and **4** were found to potently inhibit *h*DHODH indicating how the presence of a sulphur on the azole ring can effectively play a role. In particular, compound **4** is the most active compound of the all series (IC_{50} = 16 nM), being almost 24 times more potent than teriflunomide (IC_{50} = 388 nM) and only 9 times less potent than brequinar (IC_{50} = 1.8 nM) on enzymatic assay. The lower activity of compound **3** compared to compound **4** (IC_{50} 44 nM vs. 16 nM) confirms that the absence of $-OCF_3$ substituent in the second ring of the biphenylic scaffold is beneficial for the activity against *h*DHODH. Also the hydroxypyrazole moiety present in compound **5** seemed to positively interact with the binding site, being this compound more potent (IC_{50} 41 nM vs 289 nM) than hydroxyfurazan **2**. Finally, we used the hydroxytriazole system [18], to investigate the role of substituents at both N(b) and N(c) positions in inhibiting *h*DHODH. The methyl substitution is well tolerated by *h*DHODH, as compounds **6** and **7** present IC_{50} value of 45 and 18 nM, respectively. Compound **7** is the most active compound of the triazole series and comparable to the thiadiazole **4** itself. In order to obtain compounds potentially possessing a more

Table 1
Biological effects of compounds **1** – **9**, as compared to brequinar and teriflunomide. Effect of the compounds (expressed as IC_{50} value, μM, except for cytotoxicity) on [a] *h*DHODH, *in vitro* assay; [b] inhibition of cell proliferation (Jurkat T cells); [c] cytotoxicity, concentration of compounds causing a significant (≥30%) cytotoxic effect (Jurkat T cells); [d] inhibition of proliferation of PHA-stimulated PBMCs. The "n.d." notation indicates that the compound has not been tested in that specific assay.

Compound	*h*DHODH[a] IC_{50} ± SE (μM)	Proliferation[b] IC_{50} ± SE (μM)	Cytotoxicity[c] (effect≥30%)(μM)	Immuno- suppression[d] IC_{50} ± SE (μM)
Brequinar	0.0018 ± 0.0003	0.93 ± 0.08	45.0 ± 2.5	4.3 ± 0.1
Teriflunomide	0.388 ± 0.064	43.22 ± 1.24	53 ± 3	54.3 ± 3.1
1	0.599 ± 0.074	68.30 ± 7.12	>100	n.d.
2	0.289 ± 0.017	59.70 ± 3.45	>100	n.d.
3	0.044 ± 0.005	2.50 ± 0.70	5.2 ± 1.8	n.d.
4	0.016 ± 0.001	1.04 ± 0.04	78.0 ± 6.4	6.2 ± 0.4
5	0.041 ± 0.007	2.22 ± 0.13	82.0 ± 3.2	10.7 ± 0.3
6	0.045 ± 0.013	1.88 ± 0.06	>100	8.9 ± 0.7
6a	0.853 ± 0.140	13.28 ± 0.08	49.3 ± 3.4	n.d.
6b	6.0 ± 1.9	35.69 ± 0.14	56.8 ± 4.9	n.d.
7	0.018 ± 0.001	5.82 ± 0.08	8.3 ± 1.5	n.d.
8	0.108 ± 0.010	7.13 ± 0.18	11.0 ± 3.2	n.d.
9	0.036 ± 0.004	3.22 ± 0.11	6.0 ± 2.1	n.d.

promising drug-like profile, we would ideally remove two (**6a**) or three fluorine (**6b**) atoms from biphenylic scaffold of **6**. However, this modification resulted in a dramatic drop in inhibitory activity as we observed for compounds **1** and **2** on *r*DHODH [5]. In both cases, the activity profile is strictly dependent on the degree of fluorine substitution at the phenyl ring adjacent to the azole moiety. With *N*-cyclopropylmethyl analogues **8** and **9**, we intended to explore the chemical space around the N(b)/N(c) areas of the triazole ring and, at the same time, eliminate a potential metabolic liability - the *N*-methyl group, susceptible to oxidative *N*-demethylation metabolism [27]. While in the N(b) substituted analogue **8** a slight decrease in the activity was observed (if compared to its corresponding *N*-methyl substituted **6**), the N(c) substituted compound **9** maintained a good activity, although lower than its corresponding *N*-methyl substituted compound **7**. This indicates how the N(c) is better tolerated than the N(b) substitution.

2.4. Binding mode analysis of hDHODH co-crystallized in complex with compounds **4**–**6**

To evaluate experimentally the compounds binding modes and support SAR, we determined the crystal structures of *h*DHODH in complexes with the most significant inhibitors. In this sense, compounds **4**, **5** and **6**, one for each hydroxylated azole systems, were selected. The structures were determined by molecular replacement and have been refined to 1.85 Å (**4**, PDB id: 5MVC), 1.95 Å (**5,** PDB id: 5MVD) and 1.75 Å (**6**, PDB id: 5MUT**)**. X-ray data collection and refinement statistics are summarised in Table S3. The inhibitors could be clearly identified in the electron density maps in the ubiquinone binding site (Supp. Fig. S3). Superposition of *h*DHODH co-crystallized with compounds **4**–**6** shows identical binding modes for all the three inhibitors (Fig. 4). While **4** and **6** were almost superimposable, the hydroxypyrazole characterising compound **5** is posed slightly toward subsite 3, directing the 3-methyl group toward subsite 3 (Fig. 4).

In order to compare the binding mode of the three compounds with brequinar, we superposed (Fig. 5) the coordinates of co-crystallized *h*DHODH - compound **6** and co-crystallized *h*DHODH - brequinar analogue (PDB id: 1D3G) [19], previously used for the docking calculations, obtaining only few structural differences of the amino acid residues lining the ubiquinone binding site.

It can be observed how compound **6** adopts a brequinar-like [2] binding mode, placing the hydroxyl group of the heterocyclic moiety oriented toward the polar subsite 2 of the binding site (Fig. 5). The hydroxyl group was found close to the guanidine of Arg136 so that a strong interaction can be established. In addition, the hydroxy group interact through a hydrogen bond with side chain of Gln47. Notably, in brequinar the interaction with subsite 2 is guaranteed by a carboxylic group, fully deprotonated at physiological pH. However, for our active compounds, the activity seems not to be strictly associated to an high acidity of the hydroxyazole moiety; in fact comparing the pK_a of the hydroxyazoles used in design of compounds **3**–**9**, a wide range of values (3–7) [18] can be observed. In the brequinar analogue, the interaction with subsite 4 is reached by a fluorine atom present in the quinoline scaffold, positioned at distances of only 3.5 Å and 3.0 Å from Val134 and Val143 respectively [19]. In compound **6**, this role is played by a methyl group substituting the triazole ring. Being in **6** the methyl group able to reach the optimal interaction distance of 3.7 Å and 4.0 Å from Val134 and Val143 respectively, its substitution with a bulky group as is **8** could explain the observed reduced activity of this latter. In the thiadiazole **4** (Fig. 4), the sulphur atom occupies this area giving effective lipophilic interactions, as described in the literature for some thiadiazole derivatives [28,29]. In particular, the sulphur atom of compound **4** is positioned at approximately 5.0 Å and 5.5 Å from the side chains of Val134 and Val143, respectively.

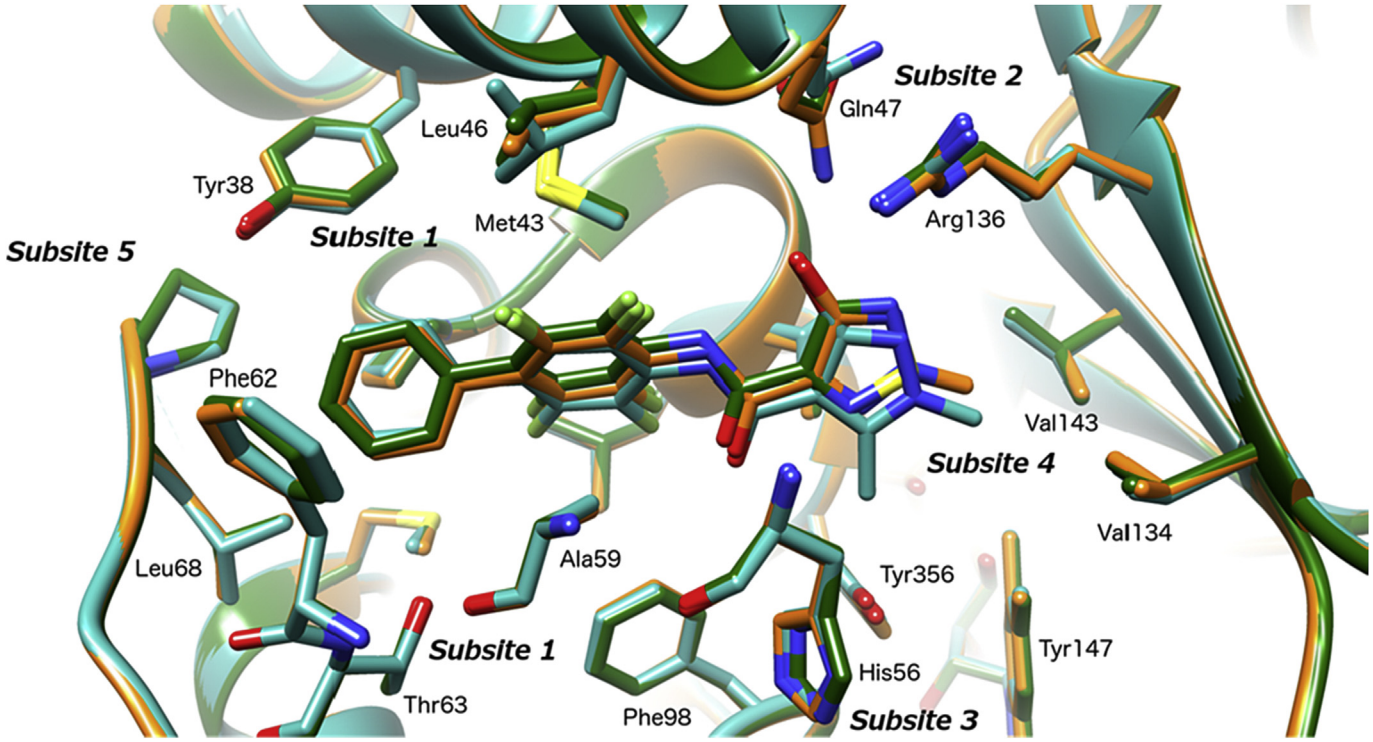

Fig. 4. Superposition of the ubiquinone binding sites from *h*DHODH co-crystallized with compounds **4** (PDB id: 5MVC, carbon atoms in green), **5** (PDB id: 5MVD, carbon atoms in light blue) and **6** (PDB id: 5MUT, carbon atoms in orange). Nitrogen, fluorine, oxygen and sulphur atoms are depicted in blue, green, red and yellow, respectively. The figure was made using PyMOL (http://www.pymol.org) [21].

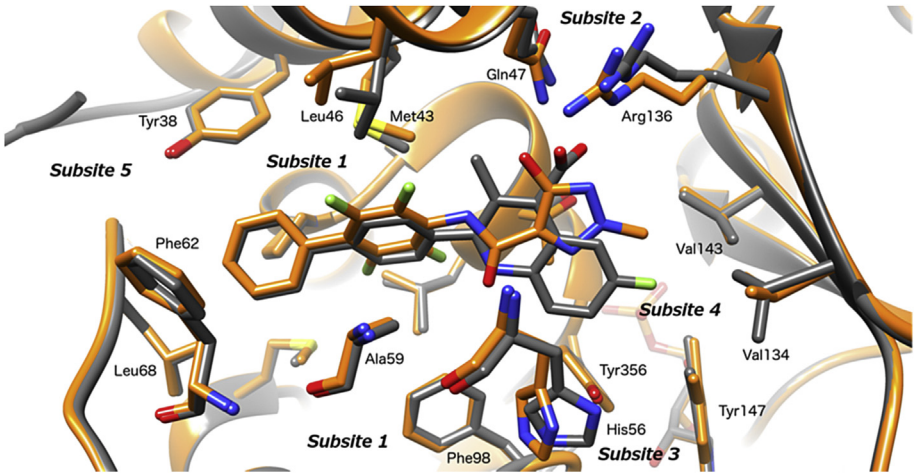

Fig. 5. Superposition of the ubiquinone binding sites from *h*DHODH co-crystallized with compound **6** (carbon atoms in orange) and a brequinar analogue (PDB id: 1D3G, carbon atoms in grey). Nitrogen, fluorine, oxygen and sulphur atoms are depicted in blue, green, red and yellow, respectively. The figure was made using PyMOL (http://www.pymol.org) [21].

The hydroxypyrazole **5** directs the 5-methyl group toward subsite 3 and the N(1)-methyl toward subsite 4 (Fig. 4), justifying its high potency (IC_{50} 41 nM). Moving to subsite 1, it can be observed how the tetrafluorinated biphenyl moiety of the three analogues (Fig. 5) occupies most of the hydrophobic pocket, in a similar manner to that of the brequinar analogue [19].

When the binding mode of **4**–**6** proposed during the docking studies (Fig. 3a,b,c) is compared with the crystallography poses (Fig. 5), only a single mayor difference can be observed. In fact, while similar interactions with subsites 1, 2, 4 are present, the carbonyl group of carboxamide function was found directed toward subsite 3 differently from docking simulation. This behaviour, similar of that observed for the brequinar-like binding pose of vidofludimus and derivatives [16], must be taken in consideration during future *hit-to-lead* optimization of the series.

2.5. Cell based assays

After evaluating compounds **1**–**9** for their ability to inhibit recombinant *h*DHODH *in vitro* we tested their effects on cell proliferation using Jurkat T cells (Table 1). Compounds **1** and **2** showed poor activity, acting as inhibitors of cell proliferation at 68.3 and 59.7 μM, respectively. On the other hand, compound **4** was as active as brequinar (1.04 versus 0.93 μM, respectively), while pyrazole **5** and some triazoles showed slightly lower activity (IC_{50} of **5** = 2.22 μM; IC_{50} of **6** = 1.88 μM). Compounds **3**–**9**, on the other hand, outperformed teriflunomide, showing 5- to 30- fold more potent antiproliferative effects (with exception of **6a** and **6b**). To evaluate whether the antiproliferative effect resulted from cell death, cytotoxicity was evaluated on Jurkat T cells using CellTox green assay, detecting the concentration of compounds able to cause 30% of cell death. Notably, compound **6** had no negative effect on cell viability even when tested at a 100 μM concentration (an induction of cell death <1% was observed); for compounds **4** and **5** cytotoxic effects were detected, although at higher concentration than for brequinar (Table 1). Compounds **7** and **9**, which had good activity in enzyme assay, showed cytotoxic behaviour already at low concentration; for this reason, they were not included in further evaluations. The same is valid for compounds **3** and **8**. Compounds **6a** and **6b** were excluded from further evaluations due to high values of IC_{50} in earlier tests.

The DHODH-dependence of antiproliferative effect of compounds **4**, **5** and **6** was tested, assaying their activity also in the presence of 100 μM uridine [30]. As shown in Fig. 6, the antiproliferative effect was reverted by the addition of exogenous uridine, strongly indicating that the compounds acted as pyrimidine biosynthesis inhibitors thereby inhibiting Jurkat cell proliferation.

Finally, to investigate the immunosuppressive activity of compounds **4**, **5** and **6**, their effect on the proliferation of phytohaemagglutinin (PHA)-activated peripheral blood mononuclear cells (PBMCs) was evaluated and compared with brequinar and teriflunomide's ones. As shown in Table 1, the antiproliferative effect of brequinar is 10 fold greater than the one showed by teriflunomide (4.3 and 54.3 μM, respectively), confirming earlier research [31–34]. All tested compounds (**4**, **5** and **6**) were found to act similarly to brequinar, inhibiting activated PBMC proliferation in the same IC_{50} range.

Order of magnitude differences were observed for activity of compounds in *h*DHODH assays and in cell based assays. This could be a consequence of different factors; poor solubility or instability of compounds during the biological tests, low membrane permeability or high unspecific protein binding. In order to exclude the first hypothesis, solubility in phosphate buffer (pH 7.4) and stability in experimental condition used for cell based assays were measured for compounds **4**–**7**, brequinar and teriflunomide (see Supporting Information). All the compounds were soluble in *h*DHODH inhibition assays as well as in cell test conditions. In this latter condition, they were also found stable (see Table S2). Therefore, other factors could reduce the cellular activity of these compounds, such as low membrane permeability or high unspecific protein binding (as in the case of brequinar [35] and teriflunomide [8]). However, investigation of these factors is beyond the intention of this work and will be a subject of following studies.

3. Conclusions

In this paper we introduced a new generation of *h*DHODH inhibitors designed by scaffold hopping replacement of the acidic moiety of brequinar with different hydroxylated azoles. All the designed compounds can potently inhibit *h*DHODH *in vitro*, reaching an IC_{50} value of 16 nM in the best example, the thiadiazole **4**. Moreover, when tested for antiproliferative activity, compounds **3**–**9** (but not **6a** and **6b**) were found to be effective in the same range of concentration as brequinar. In addition, compounds **4**, **5** and **6** have lower cellular cytotoxicity than the leads, showing cytotoxic effects at 70-fold higher concentrations than those

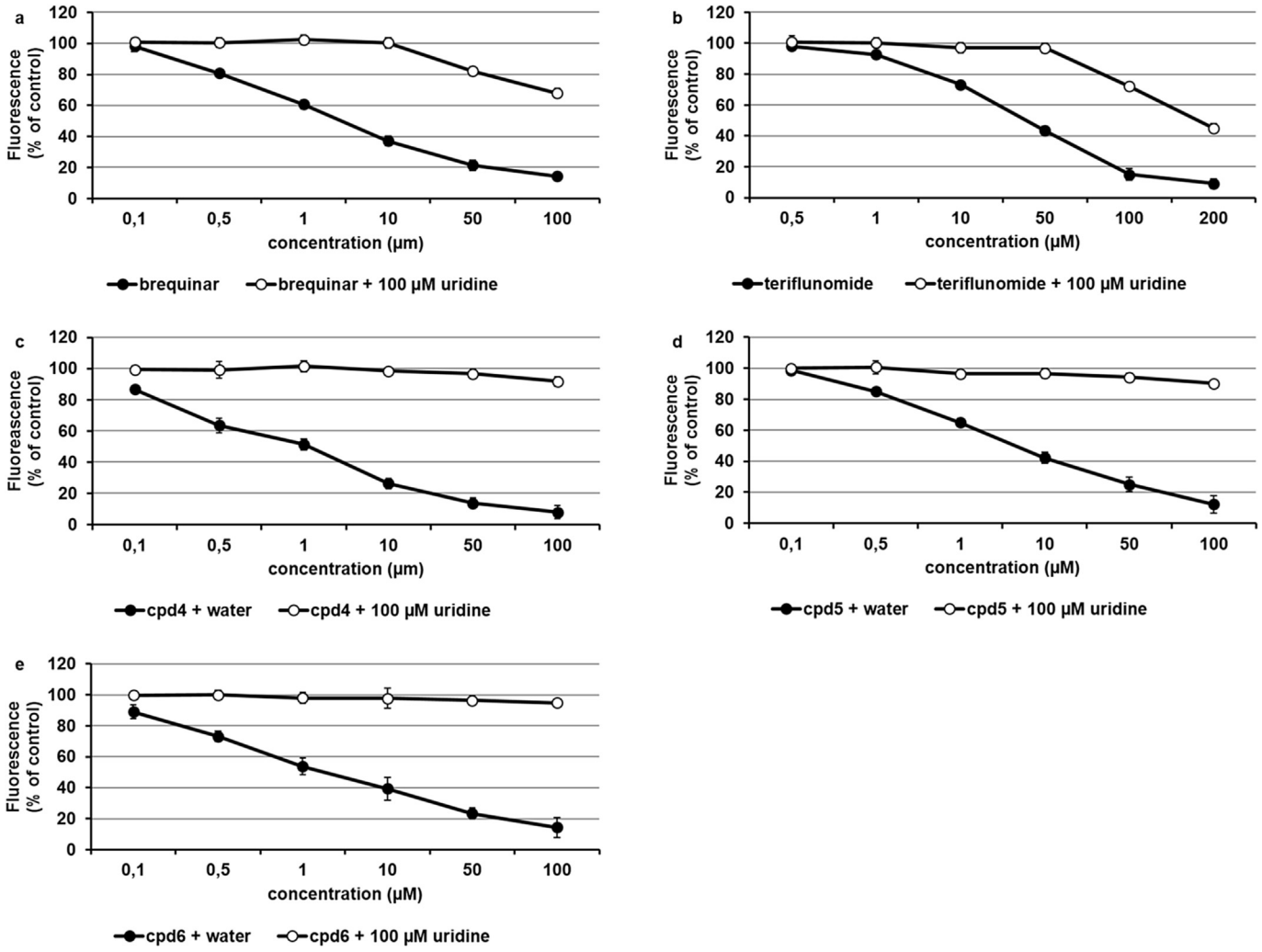

Fig. 6. The antiproliferative effect of *h*DHODH inhibitors is reverted by exogenous uridine: the antiproliferative effect of brequinar (a), teriflunomide (b), compounds **4** (c), **5** (d) and **6** (e) in the absence (black circle) or presence (empty circle) of 100 μM uridine was evaluated by quantitation of DNA content using the fluorescent dye Hoechst 33258 as described in the experimental section. Values are means of three independent experiments and are expressed as percent of DMSO-treated cells (control).

required to inhibit cell proliferation. These three promising *h*DHODH inhibitors, for which evidence suggests that antiproliferative activity depends on blocking the *de novo* pyrimidine biosynthesis, were tested for their immunosuppression activity showing promising effects on PBMC, similarly to brequinar. Compounds **4, 5** and **6** therefore represent original chemical scaffolds explored in the field of *h*DHODH inhibition and might lead to the discovery of new immunosuppressant and antiproliferative agents targeting *h*DHODH. The crystal structures of the most interesting *h*DHODH inhibitors from series **4**, **5** and **6** will facilitate subsequent optimization both in terms of drug-like properties and pharmacokinetic characteristics. In addition, optimized analogues could undergo *in vivo* tests (e.g. collagen-induced arthritis, CIA) to evaluate their anti-arthritic activity. These studies are under development and will be the subjects of forthcoming publications.

4. Experimental section

4.1. Chemistry

4.1.1. General methods

All chemical reagents were obtained from commercial sources (Sigma Aldrich, Alfa Aesar) and used without further purification. Thin-layer chromatography (TLC) was carried out to monitor the process of reactions. Analytical grade solvents (acetonitrile, diisopropyl ether, diethyl ether, dichloromethane [DCM], dimethylformamide [DMF], ethanol 99.8% v/v, ethyl acetate, methanol [MeOH], petroleum ether b.p. 40–60 °C [petroleum ether]) were used without further purification. When needed, solvents were dried on 4 Å molecular sieves. Tetrahydrofuran (THF) was distilled immediately prior to use from Na and benzophenone under N_2. Thin layer chromatography (TLC) on silica gel was carried out on 5 × 20 cm plates with 0.25 mm layer thickness. Anhydrous $MgSO_4$ was used as a drying agent for the organic phases. Purification of compounds was achieved with flash column chromatography on silica gel (Merck Kieselgel 60, 230–400 mesh ASTM) using the eluents indicated or by CombiFlash Rf 200 (Teledyne Isco) with 5–200 mL/min, 200 psi (with automatic injection valve) using RediSep Rf Silica columns (Teledyne Isco) with the eluents indicated. Compounds synthesized in our laboratory generally varied between 90% and 99% purity. The biological experiments were employed on compounds with a purity of at least 95%. Purity was checked using two analytical methods. HPLC analyses were performed on an UHPLC chromatographic system (Perkin Elmer,

Flexar). The analytical column was an UHPLC Acquity CSH Fluoro-Phenyl (2.1 × 100 mm, 1.7 μm particle size) (Waters). Compounds were dissolved in acetonitrile and injected through a 20 μL loop. The mobile phase consisted of acetonitrile/water with 0.1% trifluoroacetic acid (ratio between 60/40 and 40/60, depending on the compound's retention factor). UHPLC retention times were obtained at flow rates of 0.5 mL/min, and the column effluent was monitored at 215 and 254 nm, referenced against a 360 nm wavelength. Melting points (m.p.) were measured on a capillary apparatus (Büchi 540). The final m.p. determination was achieved by placing the sample at a temperature 10 °C below the m.p. and applying a heating rate of 1 °C min^{-1}. All compounds were routinely checked by ^{1}H- and ^{13}C NMR and mass spectrometry. IR spectra of final compounds (**3**–**9**) and their protected precursors (**15**, **16**, **21**, **31**–**36**) were recorded on FT-IR (PerkinElmer SPECTRUM BXII, KBr dispersions) using a diffuse reflectance apparatus DRIFT ACCY. MS spectra were performed on Finnigan-Mat TSQ-700 (70 eV, direct inlet for chemical ionization [CI]) or Waters Micromass ZQ equipped with ESCi source for electrospray ionization mass spectra. ^{1}H- and ^{13}C NMR spectra were performed on a Bruker Avance 300 instrument. For coupling patterns, the following abbreviations are used: br = broad, s = singlet, d = doublet, dd = doublet of doublets, t = triplet, q = quartet, m = multiplet. Chemical shifts (δ) are given in parts per million (ppm). The detailed ^{13}C spectrum of tetrafluorinated biphenyl compounds (final compounds **3**–**9** and intermediates **15**, **16**, **21**, **31**–**36**) have not been entirely reported due to their especially complicated patterns (attributable to the multiple couplings between fluorine and carbon atoms). For these spectra, only the ^{13}C signals due to heterocyclic substructure and non-aromatic carbons are indicated. Compound **18** was also checked by HSQC and HMBC 2D-NMR experiments (see Supporting Material, Figs. S1 and S2). For final compounds **3**–**9**, HRMS spectra were recorded on an LTQ Orbitrap mass spectrometer (Thermo Scientific, Bremen, Germany) equipped with an atmospheric pressure interface and an ESI ion source instrument. Compounds **1** [5], **2** [5], **10** [22], **13** [5], **14** [5], **23** and **24** [18] were prepared following already described procedures.

*4.1.1.1. 4-Benzyloxy-1,2,5-thiadiazole-3-carbonitrile **(11)**.* To a solution of compound **10** (5.00 g; 39.3 mmol) in dry DMF (60 mL) were added K_2CO_3 (6.52 g, 47.2 mmol) and benzyl bromide (4.67 mL; 39.3 mmol). The suspension was stirred for 4 h, then was quenched with water (150 mL) and extracted with diethyl ether (3 × 50 mL). The combined organic layer was washed with water and brine, dried and the solvent was evaporated under reduced pressure to afford an oily crude. This latter was then purified by flash chromatography (eluent: petroleum ether/ethyl acetate 95:5 v/v) to afford the title compound **11** as a white solid (m.p. 43.0–44.4 °C). Yield 59%. ^{1}H NMR (300 MHz, $CDCl_3$): δ 5.53 (s, 2H, CH_2), 7.40–7.53 (m, 5H, *aromatic protons*); ^{13}C NMR (75 MHz, $CDCl_3$) δ 73.5 (CH_2), 110.9 (*C*N), 122.2 (C-3), 128.5 (C*o* or C*m*), 128.7 (C*o* or C*m*), 129.0 (C*p*), 134.2 (C*ipso*), 166.3 (C-4); MS (CI) 218 (M+1).

*4.1.1.2. 4-Benzyloxy-1,2,5-thiadiazole-3-carboxylic acid **(12)**.* 2 M NaOH (17 mL) was added to a solution of **11** (2.0 g; 9.21 mmol) in MeOH (60 mL). The mixture was heated at reflux for 48 h then cooled and neutralized to pH 7 with 2 M HCl. The solution was concentrated under reduced pressure and acidified to pH 2 with 2 M HCl: the title compound **12** precipitated as a white solid (m.p. 154.6–155.5 °C; from diisopropyl ether). Yield 97%; ^{1}H NMR (300 MHz, DMSO-d_6): δ 5.49 (s, 2H, CH_2), 7.36–7.52 (m, 9H, *aromatic protons*), 13.74 (br s, 1H, O*H*); ^{13}C NMR (75 MHz, DMSO-d_6) δ 72.0 (CH_2), 127.9 (C*o* or C*m*), 128.2 (C*p*), 128.4 (C*o* or C*m*), 135.6 (C*ipso*), 140.0 (C-3), 159.9 (*C*OOH), 164.3 (C-4); MS (CI) 237 (M+1).

*4.1.1.3. 4-Benzyloxy-N-[2,3,5,6-tetrafluoro-3'-(trifluoromethoxy)[1,1'-biphenyl]-4-yl]-1,2,5-thiadiazole-3-carboxamide **(15)**.* 2 M Oxalyl chloride in dry DCM (1.59 mL, 3.18 mmol) and dry DMF (1 drop) were added to an iced solution of compound **12** (300 mg, 1.27 mmol) in dry THF (15 mL) under nitrogen atmosphere. The resulting solution was stirred at r.t. for 2 h under nitrogen atmosphere, then concentrated under reduced pressure and the residue dissolved in dry THF (10 mL, this step was repeated three times). The resulting 4-benzyloxy-1,2,5-thiadiazole-3-carbonyl chloride was dissolved in dry toluene (10 mL) under nitrogen atmosphere and added with a solution of aniline **13** (1.27 mmol, 413 mg) and dry pyridine (307 μL, 3.81 mmol) in dry toluene (5 mL). The mixture was stirred overnight at room temperature. The reaction was quenched with 0.5 M HCl (30 mL) and the layers resolved. The aqueous phase was further extracted with ethyl acetate, the combined organic layer was washed with water and brine, dried and the solvent was evaporated under reduced pressure. The crude material was purified by flash chromatography (eluent: petroleum ether/ethyl acetate 9/1 v/v) to obtain a white solid (m.p. 140.3–140.9 °C; from trituration with diisopropyl ether). Yield: 79%. ^{1}H NMR (300 MHz, $CDCl_3$): δ 5.61 (s, 2H, -OCH_2Ph), 7.35–7.57 (m, 9H, *aromatic protons*), 8.60 (s, 1H, -N*H*); ^{13}C NMR (75 MHz $CDCl_3$): δ 73.4 (-OCH_2Ph), 139.8 (C-3 of thiadiazole), 155.6 (*C*O), 163.9 (C-4 of thiadiazole); IR (KBr) ν (cm^{-1}): 3387, 1714, 1492, 1446, 1362, 1278, 1158, 992; MS (CI) 544 (M+1).

*4.1.1.4. 4-Benzyloxy-N-(2,3,5,6-tetrafluoro[1,1'-biphenyl]-4-yl)-1,2,5-thiadiazole-3-carboxamide **(16)**.* Obtained as **15**, aniline **14** was used instead of aniline **13**. White solid (m.p. 156.0–157.2 °C; from trituration with hexane). Flash chromatography eluent: petroleum ether/ethyl acetate 95:5 v/v). Yield 60%. ^{1}H NMR (300 MHz, $CDCl_3$): δ 5.60 (s, 2H, -OCH_2Ph), 7.33–7.56 (m, 10H, *aromatic protons*), 8.57 (s, 1H, -N*H*); ^{13}C NMR (75 MHz $CDCl_3$): δ 73.3 (-OCH_2Ph), 140.0 (C-3 of thiadiazole), 155.6 (*C*O), 163.9 (C-4 of thiadiazole); IR (KBr) ν (cm^{-1}): 3232, 1692, 1483, 1364, 1286, 1142, 991; MS (ESI) 460 (M+1).

*4.1.1.5. 4-Hydroxy-N-[2,3,5,6-tetrafluoro-3'-(trifluoromethoxy)[1,1'-biphenyl]-4-yl]-1,2,5-thiadiazole-3-carboxamide **(3)**.* A solution of **15** (150 mg; 0.28 mmol) in trifluoroacetic acid (20 mL) was stirred for 4 h at 70 °C. The mixture was concentrated under reduced pressure, diluted with water and extracted with ethyl acetate. The organic layer was washed with brine, dried and concentrated under reduced pressure. The crude material was purified by sequential flash chromatography (eluent: petroleum ether/ethyl acetate 8:2 v/v and DCM/MeOH/HCOOH 95:5:0.1 v/v/v) to obtain the title compound as white solid (m.p. 171.0–172.1 °C; from diisopropyl ether). Yield 50%; ^{1}H NMR (300 MHz, $CDCl_3$): δ 7.37–7.56 (m, 4H, *aromatic protons*), 8.53 (s, 1H, -N*H*), 13.09 (br s, 1H, -O*H*); ^{13}C NMR (75 MHz $CDCl_3$): δ 136.2 (C-3 of thiadiazole), 160.2 (*C*O), 165.4 (thiadiazole C-4); IR (KBr) ν (cm^{-1}): 2962, 1682, 1522, 1491, 1436, 1260, 1216, 993; ESI-HRMS (*m*/*z*) $[M - H]^-$. calcd. for $C_{16}H_5F_7N_3O_3S$ 451.9934, obsd 451.9941.

*4.1.1.6. 4-Hydroxy-N-(2,3,5,6-tetrafluoro[1,1'-biphenyl]-4-yl)-1,2,5-thiadiazole-3-carboxamide **(4)**.* Obtained as **3**, starting from **16**. Pale yellow solid (m.p. 178.7–179.9 °C; from trituration with diisopropyl ether). Yield 54%. ^{1}H NMR (300 MHz, DMSO-d_6): δ 7.31–7.82 (m, 5H, *aromatic protons*), 10.85 (s, 1H, -N*H*), 13.20 (br s, 1H, -O*H*); ^{13}C NMR (75 MHz, DMSO-d_6): δ 141.0 (C-3 of thiadiazole), 158.3 (*C*O), 164.7 (C-4 of thiadiazole); IR (KBr) ν (cm^{-1}): 3350, 1668, 1649, 1540, 1488, 1140, 990; ESI-HRMS (*m*/*z*) $[M + H]^+$ calcd. for $C_{15}H_8F_4N_3O_2S$ 370.0268, obsd. 370.0275.

*4.1.1.7. Ethyl 3-hydroxy-1,5-dimethyl-1H-pyrazole-4-carboxylate **(18)**.* Methylhydrazine (2.40 g, 52.1 mmol) was added dropwise to a cooled (0 °C) ethanol solution (45 mL) of sodium ethoxide (sodium: 2.39 g, 104 mmol) and diethyl 2-(1-ethoxyethylidene) propanedioate **17** (12.0 g, 52.1 mmol). The reaction mixture was stirred for 1 h at 0 °C and for 24 h at room temperature. 6 M HCl was added until pH 4 was reached and the resulting precipitate was isolated by filtration, washed with water and hexane, and then dried to give **18** as a white solid (m.p. 154.2–155.5 °C, after trituration with hexane; Lit [36]: 151.5–152 °C). Yield: 71%. ^{1}H NMR (300 MHz, DMSO-d_6): δ 1.23 (t, 3H, J = 7.14 Hz, -OCH$_2$C*H*$_3$), 2.38 (s, 3H, -C*H*$_3$), 3.54 (s, 3H, -NC*H*$_3$), 4.15 (q, 2H, J = 7.14 Hz, -OC*H*$_2$CH$_3$), 9.82 (br s, 1H, -O*H*). ^{13}C NMR (75 MHz, DMSO-d_6): δ 10.8 (-CH$_3$), 14.3 (-OCH$_2$CH$_3$), 35.4 (-NCH$_3$), 58.7 (-OCH$_2$CH$_3$), 95.3 (C-4), 143.1 (C-5), 160.0 (C-3), 163.2 (*C*O); MS (CI) 185 (M+1).

*4.1.1.8. Ethyl 3-(benzyloxy)-1,5-dimethyl-1H-pyrazole-4-carboxylate **(19)**.* Benzyl bromide (1.80 g, 10.6 mmol) was added dropwise to a mixture of **18** (1.77 g, 9.59 mmol) and potassium carbonate (2.65 g, 19.2 mmol) in dry DMF (20 mL). The reaction mixture was stirred for 18 h at room temperature then water (100 mL) was added. The mixture was extracted with diethyl ether (3 × 100 mL), the combined organic layer was washed with brine, dried and evaporated under reduced pressure. The residue was purified by flash chromatography (petroleum ether/ethyl acetate 8:2 v/v) to afford compound **19** as a white solid (m.p. 39.0–41.9 °C; from trituration with diisopropyl ether). Yield 75%. ^{1}H NMR (300 MHz, CDCl$_3$): δ 1.35 (t, 3H, J = 7.1 Hz, -OCH$_2$C*H*$_3$), 2.48 (s, 3H, -C*H*$_3$), 3.65 (s, 3H, -NC*H*$_3$), 4.29 (q, 2H, J = 7.1 Hz, -OC*H*$_2$CH$_3$), 5.30 (2H, *s*, -OC*H*$_2$Ph), 7.28–7.51 (m, 5H, *aromatic protons*); ^{13}C NMR (75 MHz, CDCl$_3$): δ 11.3 (-CH$_3$), 14.4 (-OCH$_2$CH$_3$), 35.8 (-NCH$_3$), 59.6 (-OCH$_2$CH$_3$), 70.0 (-OCH$_2$Ph), 97.3 (C-4), 127.0 (C*o* or *Cm*), 127.5 (C*p*), 128.3 (C*o* or *Cm*),137.2 (*Cipso*), 144.8 (C-5), 161.3, 163.7 (C-3 and CO); MS (CI) 275 (M+1).

*4.1.1.9. 3-Benzyloxy-1,5-dimethyl-1H-pyrazole-4-carboxylic acid **(20)**.* 6 M NaOH (2.40 mL, 14.2 mmol) was added to a solution of **19** (1.56 g, 5.68 mmol) in ethanol (25 mL). The mixture was stirred for 18 h at 40 °C, then neutralized with 6 M HCl. The mixture was concentrated under reduced pressure to half volume and 2 M HCl was added until a white solid precipitated (pH ~ 2). The precipitate was isolated by filtration to afford the title compound **20** as a white solid (m.p. 175.1–176.2 °C; from trituration with diisopropyl ether). Yield 90%. ^{1}H NMR (300 MHz, DMSO-d_6): δ 2.41 (s, 3H, -C*H*$_3$), 3.61 (s, 3H, -NC*H*$_3$), 5.20 (s, 2H, -OC*H*$_2$Ph), 7.31–7.46 (m, 5H, *aromatic protons*), 11.90 (s, 1H, -COO*H*); ^{13}C NMR (75 MHz, DMSO-d_6): δ 10.8 (-*C*H$_3$), 35.6 (-N*C*H$_3$), 69.2 (-O*C*H$_2$Ph), 96.4 (C-4), 127.4 (C*o* or *Cm*), 127.6 (C*p*), 128.2 (C*o* or *Cm*), 137.1 (*Cipso*), 144.6 (C-5), 160.4, 163.9 (C-3 and CO); MS (CI) 247 (M+1).

*4.1.1.10. 3-Benzyloxy-1,5-dimethyl-N-(2,3,5,6-tetrafluoro[1,1'-biphenyl]-4-yl)-1H-pyrazole-4-carboxamide **(21)**.* 2 M Oxalyl chloride in dry DCM (1.59 mL, 3.18 mmol) and dry DMF (1 drop) were added to a cooled (0 °C) solution of compound **20** (312 mg, 1.27 mmol) in dry THF (15 mL) under nitrogen atmosphere. The obtained solution was stirred at room temperature for 2 h. The solution was then concentrated under reduced pressure and the residue dissolved in dry THF (10 mL, this step was repeated three times). The resulting 3-(benzyloxy)-1,5-dimethyl-1H-pyrazole-4-carbonyl chloride was immediately used without any further purification. Trimethylaluminium (2.0 M in hexane, 0.95 mL, 1.91 mmol) was added to a solution of aniline **14** (368 mg, 1.52 mmol) in dry toluene (8 mL) under nitrogen atmosphere. The resulting mixture was stirred for 2 h at room temperature obtaining a brown suspension. This latter was quantitatively portionwise transferred to the solution of 3-(benzyloxy)-1,5-dimethyl-1H-pyrazole-4-carbonyl chloride in dry toluene (15 mL). The mixture was heated for 18 h at 80 °C, cooled to room temperature, and the reaction was quenched with 1 M HCl. The layers were resolved and the aqueous phase was exhaustively extracted with ethyl acetate. The combined organic layer was washed with 1 M NaOH and brine, dried, and the solvent was evaporated under reduced pressure. The crude product was purified by column chromatography (petroleum ether/ethyl acetate from 9:1 to 8:2) to afford the title compound **21** as a white solid (m.p. 129.3–130.4 °C; from trituration with diisopropyl ether). Yield 72%. ^{1}H NMR (300 MHz, CDCl$_3$): δ 2.59 (s, 3H, -C*H*$_3$), 3.71 (s, 3H, -NC*H*$_3$), 5.40 (s, 2H, -OC*H*$_2$Ph), 7.34–7.50 (m, 10H, *aromatic protons*), 8.38 (s, 1H, -N*H*); ^{13}C NMR (75 MHz, CDCl$_3$): δ 11.1 (-CH$_3$), 35.7 (-NCH$_3$), 71.5 (-OCH$_2$Ph), 98.2 (C-4 of the pyrazole), 145.5 (C-5 of the pyrazole), 159.3, 160.9 (C-3 of the pyrazole and CO); IR (KBr) ν (cm^{-1}): 3303, 1667, 1561, 1493, 1130, 980; MS (CI) 470 (M+1).

*4.1.1.11. Ethyl 4-benzyloxy-1-(cyclopropylmethyl)-1H-1,2,3-triazole-5-carboxylate (**26**) and 4.1.12 ethyl 5-benzyloxy-2-(cyclopropylmethyl)-2H-1,2,3-triazole-4-carboxylate (**25**).* To a solution of **22** (0.700 g, 2.83 mmol) in CH$_3$CN, K$_2$CO$_3$ (0.391 g, 2.83 mmol) and (bromomethyl)cyclopropane (0.420 g, 3.11 mmol) were added. The resulting mixture was stirred at 50 °C overnight. When the reaction was complete, the mixture was concentrated under reduced pressure; the crude product was partitioned with EtOAc (50 mL) and 1 M HCl (30 mL). The organic layer was washed with 1 M NaOH (30 mL) and brine, dried and concentrated under vacuum to afford a colorless oil. This latter showed two spots on TLC (eluent: petroleum ether/EtOAc 90/10 v/v) relative to the two triazole isomers. The mixture was separated using flash chromatography (petroleum ether/EtOAc 90/10 v/v).

(**26**) First eluted isomer, colorless oil. Yield 38%, ^{1}H NMR (300 MHz, CDCl$_3$): δ 0.43–0.48 (2H, *m*, -CH$_2$CH(C*H*$_2$)$_2$), 0.51–0.59 (2H, *m*, -CH$_2$CH(C*H*$_2$)$_2$), 1.35–1.45 (4H, *t* and *m* overlapped, -OCH$_2$C*H*$_3$ and -CH$_2$C*H*(CH$_2$)$_2$), 4.38 (2H, *q*, J = 7.1 Hz, -OC*H*$_2$CH$_3$), 4.48 (2H, *d*, J = 7.3 Hz, -C*H*$_2$CH(CH$_2$)$_2$), 5.54 (2H, *s*, -OC*H*$_2$Ph), 7.30–7.54 (5H, *m*, *aromatic protons*); ^{13}C NMR (75 MHz CDCl$_3$): δ 4.0 (-CH$_2$CH(CH$_2$)$_2$), 11.3 (-CH$_2$*C*H(CH$_2$)$_2$), 14.2 (-OCH$_2$CH$_3$), 56.2 (-NCH$_2$), 61.2 (-OCH$_2$CH$_3$), 71.5 (-OCH$_2$Ph), 110.6 (C-5), 127.6 (C*o* or *Cm*), 128.0 (C*p*), 128.4 (C*o* or *Cm*), 136.5 (*Cipso*), 158.9 (C-4), 161.1 (*C*O); MS (CI) 302 (M+1).

(**25**) Second eluted isomer, colorless oil. Yield 58%. ^{1}H NMR (300 MHz, CDCl$_3$): δ 0.37–0.47 (2H, *m*, -CH$_2$CH(C*H*$_2$)$_2$), 0.55–0.65 (2H, *m*, -CH$_2$CH(C*H*$_2$)$_2$), 1.31–1.46 (4H, *t* and *m* overlapped, -OCH$_2$C*H*$_3$ and -CH$_2$C*H*(CH$_2$)$_2$), 4.15 (2H, *d*, J = 7.3 Hz, -C*H*$_2$CH(CH$_2$)$_2$), 4.41 (2H, *q*, J = 7.1 Hz, -OC*H*$_2$CH$_3$), 5.37 (2H, *s*, -OC*H*$_2$Ph), 7.32–7.51 (5H, *m*, *aromatic protons*); ^{13}C NMR (75 MHz CDCl$_3$): δ 3.9 (-CH$_2$CH(*C*H$_2$)$_2$), 10.8 (-CH$_2$*C*H(CH$_2$)$_2$), 14.4 (-OCH$_2$*C*H$_3$), 60.6 (-NCH$_2$), 61.0 (-OCH$_2$CH$_3$), 72.2 (-OCH$_2$Ph), 123.5 (C-5), 127.7 (C*o* or *Cm*), 128.1 (C*p*), 128.4 (C*o* or *Cm*), 136.1(*Cipso*), 160.6 (*C*O or C-4), 160.7 (*C*O or C-4); MS (CI) 302 (M+1).

4.1.2. General procedure for base-catalysed ester hydrolysis

5 M NaOH (3 eq.) was added to a solution of the appropriate ester in ethanol. The solution was stirred for 2–5 h at room temperature, then neutralized with 6 M HCl and concentrated under reduced pressure. 2 M HCl was added at 0 °C until pH 2 is reached and the resulting suspension was filtered to afford the corresponding acid.

*4.1.2.1. 5-Benzyloxy-2-methyl-2H-1,2,3-triazole-4-carboxylic acid **(27)**.* Obtained from **23**, white solid (m.p. 184.5–185.8 °C; from trituration with diisopropyl ether). Yield 95%. ^{1}H NMR (300 MHz, DMSO-d_6): δ 4.07 (s, 3H, -NC*H*$_3$), 5.29 (s, 2H, -OC*H*$_2$Ph), 7.35–7.47

(m, 5H, *aromatic protons*), 12.92 (s, 1H, -COO*H*); ^{13}C NMR (75 MHz DMSO-d_6): δ 43.4 (-NCH$_3$), 71.7 (-OCH$_2$Ph), 123.4 (C-4), 127.9 (C*o* or *Cm*), 128.0 (C*p*), 128.2 (C*o* or *Cm*), 135.9 (C*ipso*), 159.9, 160.7 (C-5 and CO); MS (ESI) 234 (M+1).

*4.1.2.2. 4-Benzyloxy-1-methyl-1H-1,2,3-triazole-5-carboxylic acid **(28)**.* Obtained from **24**, white solid (m.p. 186.5–187.7 °C, from trituration with diisopropyl ether). Yield 95%. ^{1}H NMR (300 MHz, DMSO-d_6): δ 4.15 (s, 3H, -NC*H*$_3$), 5.43 (s, 2H, -OC*H*$_2$Ph), 7.33–7.48 (m, 5H, *aromatic protons*), 13.58 (br s, 1H, -COO*H*); ^{13}C NMR (75 MHz, DMSO-d_6): δ 39.5 (-NCH$_3$), 71.8 (-OCH$_2$Ph), 112.8 (C-5), 128.7 (C*o* or *Cm*), 129.0 (C*p*), 129.2 (C*o* or *Cm*), 137.4 (C*ipso*), 160.1, 161.2 (C-4 and CO); MS (ESI) 234 (M+1).

*4.1.2.3. 5-Benzyloxy-2-(cyclopropylmethyl)-2H-1,2,3-triazole-4-carboxylic acid **(29)**.* Obtained from **25**, white solid (m.p. 157.8–159.3; from trituration with diisopropyl ether). Yield 85%. ^{1}H NMR (300 MHz, DMSO-d_6): δ 0.37–0.42 (m, 2H, -CH$_2$CH(C*H*$_2$)$_2$), 0.52–0.58 (m, 2H, -CH$_2$CH(C*H*$_2$)$_2$), 1.22–1.36 (m, 1H, -CH$_2$C*H*(CH$_2$)$_2$), 4.19 (d, 2H, *J* = 7.3 Hz, -C*H*$_2$CH(CH$_2$)$_2$), 5.30 (s, 2H, -OC*H*$_2$Ph), 7.32–7.52 (m, 5*H*, *aromatic protons*), 12.95 (br s, 1H, -COO*H*); ^{13}C NMR (75 MHz, DMSO-d_6): δ 3.5 (-CH$_2$CH(*C*H$_2$)$_2$), 10.5 (-CH$_2$CH(CH$_2$)$_2$), 59.5 (-NCH$_2$), 71.6 (-OCH$_2$Ph), 123.2 (C-4), 128.0 (C*o* or *Cm*), 128.1 (C*p*), 128.3 (C*o* or *Cm*), 136.0 (C*ipso*), 159.9, 161.0 (C-5 and CO); MS (CI) 274 (M+1).

*4.1.2.4. 4-Benzyloxy-1-(cyclopropylmethyl)-1H-1,2,3-triazole-5-carboxylic acid **(30)**.* Obtained from **26**, white solid (m.p. 167.4–168.2, from trituration with diisopropyl ether). Yield 93%. ^{1}H NMR (300 MHz, DMSO-d_6): δ 0.31–0.59 (m, 4H, -CH$_2$CH(C*H*$_2$)$_2$), 1.23–1.38 (m, 1H, -CH$_2$C*H*(CH$_2$)$_2$), 4.43 (d, 2H, *J* = 7.3 Hz, -C*H*$_2$CH(CH$_2$)$_2$), 5.44 (s, 2H, -OC*H*$_2$Ph), 7.32–7.50 (m, 5H, *aromatic protons*), 13.64 (br s, 1H, -COO*H*); ^{13}C NMR (75 MHz, DMSO-d_6): δ 3.5 (-CH$_2$CH(*C*H$_2$)$_2$), 11.2 (-CH$_2$*C*H(CH$_2$)$_2$), 55.1 (-NCH$_2$), 70.8 (OCH$_2$Ph), 110.8 (C-5), 127.8 (C*o* or *Cm*), 128.0 (C*p*), 128.3 (C*o* or *Cm*), 136.4 (C*ipso*), 159.2, 160.2 (C-4 and CO); MS (CI) 274 (M+1).

*4.1.3. General procedure for synthesis of triazole related amides **31**–**36***

2 M oxalyl chloride in dry DCM (1.75 mL, 3.50 mmol) and dry DMF (1 drop) were added to a cooled (0 °C) solution of the specific carboxylic acid (1.00 mmol) in dry THF (15 mL) under nitrogen atmosphere. The reaction mixture was stirred for 2 h at room temperature under nitrogen atmosphere. The solution was concentrated under reduced pressure and the residue was dissolved in dry THF (10 mL, this step was repeated three times). The resulting acyl chloride was dissolved in dry toluene (15 mL). A solution of the appropriate aniline (1.00 mmol) and dry pyridine (3.00 mmol) in dry toluene (5 mL) was added dropwise to the solution of acyl chloride under nitrogen atmosphere. The resulting mixture was stirred at reflux overnight, then cooled to room temperature and quenched with 0.5 M HCl (25 mL). The layers were resolved, the aqueous phase was further extracted with ethyl acetate, the combined organic layer was washed with brine, dried and evaporated under reduced pressure. The crude material was purified by flash chromatography.

*4.1.3.1. 5-Benzyloxy-2-methyl-N-(2,3,5,6-tetrafluoro[1,1'-biphenyl]-4-yl)-2H-1,2,3-triazole-4-carboxamide **(31)**.* Obtained from **27**, using aniline **15.** Flash chromatography eluent: petroleum ether/ethyl acetate from 9:1 to 8:2 v/v). White solid (m.p. 147.6–148.2 °C; from trituration with hexane). Yield 60%. ^{1}H NMR (300 MHz, CDCl$_3$): δ 4.15 (s, 3H, -NC*H*$_3$), 5.43 (s, 2H, -OC*H*$_2$Ph), 7.32–7.56 (m, 10H, *aromatic protons*), 8.08 (s, 1H, -N*H*); ^{13}C NMR (75 MHz CDCl$_3$): δ 42.7 (-NCH$_3$), 73.3 (-OCH$_2$Ph), 125.2 (C-4 of the triazole), 157.1, 159.2 (C-5 of the triazole and CO); IR (KBr) ν (cm^{-1}): 3228, 1678, 1527, 1492, 1167, 988; MS (ESI) 457 (M+1).

*4.1.3.2. 5-(Benzyloxy)-N-(3,5-difluoro[1,1'-biphenyl]-4-yl)-2-methyl-2H-1,2,3-triazole-4-carboxamide **(32)**.* Obtained from **27**, using 3,5-difluoro[1,1'-biphenyl]-4-amine. Flash chromatography eluent: petroleum ether/ethyl acetate 80:20 v/v. White solid (m.p. 148.8–149.8 °C). Yield 94%. ^{1}H NMR (300 MHz, CDCl$_3$): δ 4.14 (s, 3H, -NC*H*$_3$), 5.43 (s, 2H, -OC*H*$_2$Ph), 7.17–7.23 (m, 2H, *aromatic protons*), 7.34–7.54 (m, 10H, *aromatic protons*), 8.01 (s, 1H, -N*H*); ^{13}C NMR (75 MHz CDCl$_3$): δ 42.6 (-NCH$_3$), 73.1 (OCH$_2$Ph), 110.4 (dd, *J* = 22.3, 2.1 Hz), 112.1 (t, *J* = 16.8 Hz), 125.6 (C-4 of the triazole), 126.9, 128.0, 128.5, 128.6, 128.7, 129.1, 135.4, 138.6 (*aromatic carbons*), 141.4 (t, *J* = 9.3 Hz), 157.3 (C-5 of the triazole or CO), 157.9 (dd, *J* = 250.6, 5.7 Hz), 159.1 (C-5 of the triazole or CO); IR (KBr) ν (cm^{-1}): 3366, 3054, 1682, 1551, 1531, 1450, 1120, 1038; MS (ESI) 421 (M+1).

*4.1.3.3. 5-(Benzyloxy)-N-(3-fluoro[1,1'-biphenyl]-4-yl)-2-methyl-2H-1,2,3-triazole-4-carboxamide **(33)**.* Obtained from **27**, using 3-fluoro [1,1'-biphenyl]-4-amine. Flash chromatography eluent: petroleum ether/ethyl acetate 80:20 v/v. White solid (m.p. 170.4–172.1 °C). Yield 70%. ^{1}H NMR (300 MHz, CDCl$_3$): δ 4.13 (s, 3H, -NC*H*$_3$), 5.43 (s, 2H, -OC*H*$_2$Ph), 7.30–7.45 (m, 8H, *aromatic protons*), 7.50–7.57 (m, 4H, *aromatic protons*), 8.59 (t, *J* = 8.4 Hz, 1H, *aromatic proton*), 8.81 (s, 1H, -N*H*); ^{13}C NMR (75 MHz CDCl$_3$): δ 42.6 (-NCH$_3$), 73.2 (-OCH$_2$Ph), 113.2 (d, *J* = 19.9 Hz), 121.7 (d, *J* = 1.4 Hz), 123.1 (d, *J* = 3.1 Hz), 125.5 (d, *J* = 10.2 Hz) (*aromatic carbons*), 126.2 (C-4 of the triazole), 126.8, 127.6, 128.2, 128.2, 128.7, 128.9, 135.2, 137.4 (d, *J* = 7.2 Hz), 139.5 (d, *J* = 2.1 Hz), 152.4 (d, *J* = 242.1 Hz), 157.3 (*aromatic carbons*), 158.6 (C-5 of the triazole and CO); IR (KBr) ν (cm^{-1}): 3368, 1690, 1598, 1532, 1309, 1148, 956; MS (ESI) 403 (M+1).

*4.1.3.4. 4-Benzyloxy-1-methyl-N-(2,3,5,6-tetrafluoro[1,1'-biphenyl]-4-yl)-1H-1,2,3-triazole-5-carboxamide **(34)**.* Obtained from **28**, using aniline **15.** Flash chromatography eluent: petroleum ether/ethyl acetate 9:1 v/v). White solid (m.p. 145.0–145.9 °C; from trituration with hexane). Yield 56%. ^{1}H NMR (300 MHz, CDCl$_3$): δ 4.34 (s, 3H, -NC*H*$_3$), 5.65 (s, 2H, -OC*H*$_2$Ph), 7.32–7.60 (m, 10H, *aromatic protons*), 8.27 (s, 1H, -N*H*); ^{13}C NMR (75 MHz CDCl$_3$): δ 38.9 (-NCH$_3$), 73.1 (-OCH$_2$Ph), 112.6 (C-5 of the triazole), 155.4, 159.1 (C-4 of the triazole and CO); IR (KBr) ν (cm^{-1}): 3348, 1704, 1532, 1493, 1439, 1141, 991; MS (ESI) 457 (M+1).

*4.1.3.5. 5-Benzyloxy-2-(cyclopropylmethyl)-N-(2,3,5,6-tetrafluoro[1,1'-biphenyl]-4-yl)-2H-1,2,3-triazole-4-carboxamide **(35)**.* Obtained from **29**, using aniline **15.** Flash chromatography eluent: petroleum ether/ethyl acetate 9:1 v/v. White solid (m.p. 123.8–125.1 °C; from trituration with hexane). Yield 53%. ^{1}H NMR (300 MHz, CDCl$_3$): δ 0.45–0.50 (m, 2H, -CH$_2$CH(C*H*$_2$)$_2$), 0.63–0.69 (m, 2H, -CH$_2$CH(C*H*$_2$)$_2$), 1.37–1.47 (m, 1H, -CH$_2$C*H*(CH$_2$)$_2$), 4.20 (d, 2H, *J* = 7.3 Hz, -C*H*$_2$CH(CH$_2$)$_2$), 5.45 (s, 2H, -OC*H*$_2$Ph), 7.36–7.52 (m, 10H *aromatic protons*), 8.11 (s, 1H, -N*H*); ^{13}C NMR (75 MHz CDCl$_3$): δ 4.0 (-CH$_2$CH(*C*H$_2$)$_2$), 10.8 (-CH$_2$*C*H(CH$_2$)$_2$), 60.8 (-NCH$_2$), 73.2 (-OCH$_2$Ph), 124.9 (C-4 of the triazole), 157.3, 159.1 (C-5 of the triazole and CO); IR (KBr) ν (cm^{-1}): 3242, 1682, 1536, 1491, 1464, 1162, 988; MS (CI) 497 (M+1).

*4.1.3.6. 4-Benzyloxy-1-(cyclopropylmethyl)-N-(2,3,5,6-tetrafluoro[1,1'-biphenyl]-4-yl)-1H-1,2,3-triazole-4-carboxamide **(36)**.* Obtained from **30**, using aniline **15.** Flash chromatography eluent: petroleum ether/ethyl acetate 95:5 v/v. White solid (m.p. 124.5–125.7 °C; from trituration with hexane). Yield 70%. ^{1}H NMR (300 MHz, CDCl$_3$): δ 0.42–0.65 (m, 4H, -CH$_2$CH(C*H*$_2$)$_2$), 1.39–1.58 (m, 1H -CH$_2$C*H*(CH$_2$)$_2$), 4.61 (d, 2H, *J* = 7.3 Hz, -C*H*$_2$CH(CH$_2$)$_2$), 5.66

(s, 2H, -OCH_2Ph), 7.34–7.60 (m, 10H, *aromatic protons*), 8.34 (s, 1H, -N*H*); ^{13}C NMR (75 MHz $CDCl_3$): δ 4.0 (-CH_2CH(CH_2)$_2$), 11.4 (-CH_2CH(CH_2)$_2$), 56.4 (-NCH_2), 73.1 (-OCH_2Ph), 111.7 (C-5 of the triazole), 155.3, 159.2 (C-4 of the triazole and CO); IR (KBr) ν (cm^{-1}): 3270, 1676, 1628, 1522, 1463, 1151, 990; MS (ESI) 497 (M+1).

4.1.4. General hydrogenation procedure to obtain target compounds 5–9

Palladium on carbon (Pd/C, 45 mg) was added to a solution of the appropriate amide (compounds **21**, **31**–**36**, 0.300 mmol) in dry THF (15 mL). The resulting mixture was vigorously stirred under hydrogen atmosphere for 1 h. The suspension was filtered through Celite, washing the cake with methanol. The filtrate was concentrated under reduced pressure. When necessary, the obtained solid was further purified by flash chromatography.

4.1.4.1. 3-Hydroxy-1,5-dimethyl-N-(2,3,5,6-tetrafluoro[1,1'-biphenyl]-4-yl)-1H-pyrazole-4-carboxamide ***(5)***. White solid (m.p. 273.0–275.1 °C; from trituration with diisopropyl ether). Yield 93%. ^{1}H NMR (300 MHz, DMSO-d_6): δ 2.47 (s, 3H, -CH_3), 3.59 (s, 3H, -NCH_3), 7.66–7.47 (m, 5H, *aromatic protons*), 9.17 (br s, 1H, -N*H*); ^{13}C NMR (75 MHz DMSO-d_6): δ 10.5 (-CH_3), 34.9 (-NCH_3), 96.7 (C-4 of pyrazole), 144.4 (C-5 of pyrazole), 159.1, 160.8 (C-3 of pyrazole and CO); IR (KBr) ν (cm^{-1}): 3344, 1682, 1523, 1438, 1134, 984; ESI-HRMS (*m*/*z*) [M + H]$^+$ calcd. for $C_{18}H_{14}F_4N_3O_2$ 380.1017, obsd. 380.1024.

4.1.4.2. 5-Hydroxy-2-methyl-N-(2,3,5,6-tetrafluoro[1,1'-biphenyl]-4-yl)-2H-1,2,3-triazole-4-carboxamide ***(6)***. Flash chromatography eluent: DCM/methanol from 99:1 to 9:1 v/v). White solid (m.p. 230.2–231.1 °C; from trituration with diisopropyl ether). Yield 98%. ^{1}H NMR (300 MHz, DMSO-d_6): δ 4.08 (s, 3H, -NCH_3), 7.55–7.57 (m, 5H, *aromatic protons*), 10.23 (br s, 1H, -N*H*), 11.36 (br s, 1H, -O*H*); ^{13}C NMR (DMSO-d_6): δ 43.0 (-NCH_3), 124.71 (C-4 of the triazole), 159.3, 160.2 (C-5 of the triazole and (CO); IR (KBr) ν (cm^{-1}): 3390, 3356, 1672, 1559, 1527, 1490, 1147, 988; ESI-HRMS (*m*/*z*) [M + H]$^+$ calcd. for $C_{16}H_{11}F_4N_4O_2$ 367.0813, obsd. 367.0815.

4.1.4.3. N-(3,5-Difluoro[1,1'-biphenyl]-4-yl)-5-hydroxy-2-methyl-2H-1,2,3-triazole-4-carboxamide ***(6a)***. Flash chromatography eluent: DCM/methanol 90:10 v/v. White solid (m.p. 224.0–224.7 °C. Yield 95%. ^{1}H NMR (300 MHz, DMSO-d_6): δ 4.05 (s, 3H, -NCH_3), 7.40–7.56 (m, 5H, *aromatic protons*), 7.76 (d, J = 7.1 Hz, 2H), 9.67 (s, 1H, -N*H*), 11.37 (br s, 1H, -O*H*); ^{13}C NMR (DMSO-d_6): δ 42.2 (-NCH_3), 109.9 (dd, J = 23.5, 1.3 Hz), 113.2 (t, J = 17.2 Hz) (*aromatic carbons*), 124.3 (C-4 of the triazole), 126.8, 128.6, 129.1, 137.5 (t, J = 2.2 Hz), 140.5 (t, J = 9.7 Hz), 158.6 (dd, J = 248.2, 6.1 Hz), 158.7 (*aromatic carbons*), 158.8 (C-5 of the triazole and CO); IR (KBr) ν (cm^{-1}): 3409, 3338, 1659, 1556, 1416, 1132, 1038; MS (ESI) 331 (M+1). ESI-HRMS (*m*/*z*) [M + H]$^+$ calcd. for $C_{16}H_{13}F_2N_4O_2$ 331.1001, obsd. 331.1000.

4.1.4.4. N-(3-Fluoro[1,1'-biphenyl]-4-yl)-5-hydroxy-2-methyl-2H-1,2,3-triazole-4-carboxamide ***(6b)***. Flash chromatography eluent: DCM/methanol 90:10 v/v. White solid (m.p. 214.9–215.8 °C. Yield 97%. ^{1}H NMR (300 MHz, DMSO-d_6): δ 4.05 (s, 3H, -NCH_3), 7.36 (m, 1H), 7.46 (t, J = 7.4 Hz, 2H), 7.55 (d, J = 8.4 Hz, 1H), 7.76–7.60 (m, 3H), 8.18 (t, J = 8.4 Hz, 1H) (*aromatic protons*), 9.45 (s, 1H, -N*H*), 12.22 (br s, 1H, -O*H*); ^{13}C NMR (DMSO-d_6): δ 43.1 (-NCH_3), 113.4 (d, J = 20.4 Hz), 122.6 (d, J = 3.0 Hz), 123.4 (d, J = 1.9 Hz), 124.9 (C-4 of the triazole), 125.2 (d, J = 11.3 Hz), 126.5, 127.8, 129.0, 137.1 (d, J = 7.4 Hz), 138.4 (d, J = 2.0 Hz), 153.5 (d, J = 243.7 Hz), 157.8, 158.1 (C-5 of the triazole and CO); IR (KBr) ν (cm^{-1}): 3409, 3373, 1666, 1560, 1558, 1538, 1145; MS (ESI) 313 (M+1). ESI-HRMS (*m*/*z*) [M + H]$^+$ calcd. for $C_{16}H_{14}F_1N_4O_2$ 313.10953, obsd. 313.1094.

4.1.4.5. 4-Hydroxy-1-methyl-N-(2,3,5,6-tetrafluoro[1,1'-biphenyl]-4-yl)-1H-1,2,3-triazole-5-carboxamide ***(7)***. Flash chromatography eluent: petroleum ether/ethyl acetate 7:3 v/v, then DCM/methanol 95:5 v/v). White solid (m.p. 247.9–248.5 °C with decomposition; from trituration with diisopropyl ether). Yield 99%. ^{1}H NMR (300 MHz, DMSO-d_6): δ 4.16 (s, 3H, -NCH_3), 7.53–7.60 (m, 5H, *aromatic protons*), 9.86 (br s, 1H, -N*H*); ^{13}C NMR (DMSO-d_6): δ 39.4 (-NCH_3), 110.4 (C-5 of the triazole), 156.5, 160.5 (C-4 of the triazole and CO); IR (KBr) ν (cm^{-1}): 3000, 1699, 1640, 1537, 1488, 1439, 1153, 988; ESI-HRMS (*m*/*z*) [M + H]$^+$ calcd. for $C_{16}H_{11}F_4N_4O_2$ 367.0813, obsd. 367.0812.

4.1.4.6. 2-(Cyclopropylmethyl)-5-hydroxy-N-(2,3,5,6-tetrafluoro[1,1'-biphenyl]-4-yl)-2H-1,2,3-triazole-4-carboxamide ***(8)***. Pale yellow solid (m.p. 158.3–159.1 °C; from trituration with diisopropyl ether). Yield 88%. ^{1}H NMR (300 MHz, DMSO-d_6): δ 0.38–0.48 (m, 2H, -CH_2CH(CH_2)$_2$), 0.53–0.65 (m, 2H, -CH_2CH(CH_2)$_2$), 1.26–1.42 (m, 1H -CH_2CH(CH_2)$_2$), 4.20 (d, 2H, J = 7.3 Hz, -CH_2CH(CH_2)$_2$), 7.45–7.66 (m, 5H, *aromatic protons*), 10.04 (br s, 1H, -N*H*), 11.59 (br s, 1H, -O*H*); ^{13}C NMR (DMSO-d_6): δ 3.7 (-CH_2CH(CH_2)$_2$), 10.7 (-CH_2CH(CH_2)$_2$), 59.5 (-NCH_2), 123.9 (C-4 of the triazole), 158.4, 158.8 (C-5 of the triazole and CO); IR (KBr) ν (cm^{-1}): 3393, 1671, 1551, 1494, 1144, 987; ESI-HRMS (*m*/*z*) [M + H]$^+$ calcd. for $C_{19}H_{15}F_4N_4O_2$ 407.1126, obsd. 407.1134.

4.1.4.7. 1-(Cyclopropylmethyl)-4-hydroxy-N-(2,3,5,6-tetrafluoro[1,1'-biphenyl]-4-yl)-1H-1,2,3-triazole-5-carboxamide ***(9)***. Flash chromatography eluent: petroleum ether/ethyl acetate 8:2 v/v, then DCM/methanol 95:5 v/v). White solid (m.p. 200.1–200.9 °C with decomposition; from hexane). Yield 92%. ^{1}H NMR (300 MHz, DMSO-d_6): δ 0.33–0.45 (m, 2H, -CH_2CH(CH_2)$_2$), 0.46–0.57 (m, 2H, -CH_2CH(CH_2)$_2$), 1.27–1.40 (m, 1H -CH_2CH(CH_2)$_2$), 4.46 (d, 2H, J = 7.3 Hz, -CH_2CH(CH_2)$_2$), 7.54–7.59 (m, 5H, *aromatic protons*), 9.73 (br s, 1H, -N*H*), 13.15 (br s, 1H, -O*H*); ^{13}C NMR (DMSO-d_6): δ 3.4 (-CH_2CH(CH_2)$_2$), 11.2 (-CH_2CH(CH_2)$_2$), 54.8 (-NCH_2), 109.9 (C-5 of the triazole), 156.1, 159.1 (C-4 of the triazole and CO); IR (KBr) ν (cm^{-1}): 2924, 1693, 1643, 1513, 1490, 1096, 989; ESI-HRMS (*m*/*z*) [M + H]$^+$ calcd. for $C_{19}H_{15}F_4N_4O_2$ 407.1126, obsd. 407.1129.

4.2. Molecular modelling

The structures of compounds **1**–**9**, as well as the structures of the lead compounds teriflunomide and brequinar, were built in their dissociated forms using the 2D Sketcher tool implemented in Maestro GUI. For each compound, a Monte-Carlo Multiple Minimum (MCMM) conformational search was performed using MacroModel. Quantum mechanics/molecular mechanics (QM/MM) docking was performed using Schrödinger QM-Polarized Ligand Docking protocol (QPLD) [37]. For this purpose, the crystal structure with PDB id:1D3G [19] and the generated conformers were docked. Before docking, the crystal structure of the protein underwent an optimization process using the Protein Preparation Wizard tool, implemented in Maestro™ GUI. Missing hydrogen atoms were added and bond orders were assigned while missing loops and residues not belonging to the binding site were capped by adding ACE (*N*-acetyl) and NMA (N-methylamide) groups. Then, ORO, non-structural water molecules and impurities (such as solvent molecules) were removed. Only the cofactor FMN and the co-crystalized ligand brequinar analogue were maintained. Reorienting automatically optimized the hydrogen bond network: hydroxyl and thiol groups, amide groups of Asn and Gln, and the imidazole ring in His. Moreover, the protonation states prediction of His—Asp, Glu, and tautomeric states of His—were accomplished using PROPKA.™ Finally, a restrained minimization of the protein structure was accomplished by converging heavy atoms to a 0.30 Å RMSD. A grid

of 10 Å × 10 Å x 10 Å (*x*, *y*, and *z*) was created and centered on the co-crystalized ligand brequinar analogue. The ligand was extracted from the structure and used for docking validation. The QPLD protocol was carried out using Glide Extra Precision (XP) mode, setting QM Level to Accurate (B3LYP functional, 6-31G*/LACVP* basis set, ultrafine SCF accuracy level). In the QPLD procedure, after the first XP docking run, QM-derived charge is calculated for the top five poses of each compound in the field of the receptor. Then, a new XP docking is performed with new QM charges calculated. Finally, re-docking and re-scoring were performed, keeping the 10 highest ranked poses.

4.3. Protein expression and purification for enzyme assay

The cDNA of the *N*-terminal truncated form of *h*DHODH (aa31 - 395) was amplified from full length *h*DHODH I.M.A.G.E. clone (ID 6064723) and inserted into a pFN2A vector (Promega). The vector produces *h*DHODH as an *N*-terminal GST-fusion protein. The plasmid pFN2A–*h*DHODH was transformed into BL21 (DE3) pyrD *Escherichia coli* cells for protein production. Cells were grown at 37 °C in LB medium supplemented with 0.1 mM flavin mononucleotide. After 20 h of growth, cells were induced with 0.4 mM isopropyl-D-thiogalactopyranoside at an OD_{600} of 0.6–0.8 at 28 °C for an additional 3 h. A cell pellet from 300 mL of culture was lysed in 20 mL of PBS (50 mM Na_2HPO_4, 50 mM NaH_2PO_4, 500 mM NaCl) supplemented with 24 mg lysozyme and 0.2% v/v protease inhibitor cocktail (Sigma-Aldrich), incubated 30 min on ice, and disrupted by sonication. Triton X-100 was added to a final concentration of 1% into the lysate before centrifugation at 14000 × g for 40 min at 4 °C. The clarified supernatant was incubated with DNase I (Sigma Aldrich) for 30 min at room temperature, supplemented with 2 mM DTT, and filtered through a 0.45 μm syringe filter. The GST-fused enzyme was purified from bacterial lysate by affinity chromatography on immobilized glutathione-sepharose columns using fast protein liquid chromatography (FPLC). The GST tag was not removed for further studies.

4.4. hDHODH inhibition assay

Inhibitory activity was assessed by monitoring the reduction of 2,6-dichloroindophenol (DCIP), which is associated with oxidation of dihydroorotate catalyzed by the DHODH enzyme. The enzyme was pre-incubated for five minutes at 37 °C in Tris-buffer solution (pH 8.0) with coenzyme Q10 (100 μM), tested compounds at different concentrations (final DMSO concentration 0.1% v/v), and DCIP (50 μM). The reaction was initiated by addition of DHO (500 μM) and the reduction was monitored at λ = 650 nm. The initial rate was measured in the first five minutes (ε = 10400 M-1cm-1) and an IC_{50} value was calculated [38] using GraphPad Prism software. Values are means ± SE of three independent experiments.

4.5. Cell culture and drug treatments

Jurkat cells were cultured in X-VIVO 15 (BE02-060F, Lonza) supplemented with 10% (v/v) fetal bovine serum (F-7524, Sigma Aldrich) and 1% (v/v) antibiotic-antimycotic solution (A-5955, Sigma Aldrich) (complete medium). Cells were maintained at 37 °C in a 5% CO_2 humidified atmosphere.

Cells were passaged every 2–3 days and discarded after 15 passages. Jurkat cells were routinely tested to confirm the absence of Mycoplasma using MycoAlert Plus detection kit (Lonza) and were used between passages 5 and 10 for all experiments. Jurkat cell line was authenticated by short tandem repeat profiling (Microsynth, Balgach, Switzerland) and found to match repository samples in 100% of tested alleles. ATCC (www.atcc.org), DSMZ (www.dsmz.de) STR databases were used to check the authenticity of the cell line.

Each compound tested was solubilized in DMSO (drug vehicle, 41639, Fluka) at a final concentration of 10 mM, which was used as the stock solution for all experiments. Final dilutions were made in culture medium.

4.6. Proliferation assay

Growth of Jurkat T-cells was evaluated by quantitation of DNA content using the fluorescent dye Hoechst 33258 [39]. Cells (5×10^3 in 100 μL medium) were seeded in a white 96-well plate and exposed to increasing concentrations (0.001–200 μM) of each compound or vehicle (DMSO) for 72 h. At the end of incubation, medium was aspirated and the wells washed twice with 100 μL phosphate buffer saline (137 mM NaCl, 2.7 mM KCl, 8.1 mM Na_2HPO_4, 1.76 mM KH_2PO_4, PH 7.4). Cells were exposed to 100 μL 0.02% SDS solution in SSC buffer (154 mM NaCl, 15 mM sodium citrate, pH 7) for 1 h at 37 °C with occasional swirling. At the end, an equal volume of 1 μg/mL Hoechst 33258 solution in SSC buffer was added to each well and fluorescence measured at 355 nm (excitation) and 460 nm (emission) using a Fluoroskan Ascent-Thermo microplate fluorometer (Thermo Fisher Scientific, MA). IC_{50} values were determined using nonlinear regression plots with GraphPad Prism6. Values are means ± SE of three independent experiments. Where indicated, the antiproliferative effect was evaluated in the presence of 100 μM uridine [30].

4.7. Immunosuppression assay

PBMCs were isolated by Ficoll/Isopaque (Lymphoprep) density gradient centrifugation of buffy coat leukopheresis residues from fresh blood samples from healthy donors. Purified cells were grown and maintained in culture medium at 37 °C in 5% CO_2 humidified atmosphere. Cell proliferation was assessed as BrdU incorporation in newly synthesized DNA using a chemiluminescent ELISA assay (Roche). Cells (5×10^3/well) were seeded in a white-opaque 96-well plate and exposed to increasing concentrations (0.001–200 μM) of each compound or vehicle (DMSO) for 2 h and then stimulated with 1.25 mg/mL phytohaemagglutinin (PHA) for 72 h. BrdU label was added at a final concentration of 10 μM for the last 16 h. IC_{50} values were determined using nonlinear regression plots with GraphPad Prism6. Values are means ± SE of three independent experiments.

4.8. Cytotoxicity assay

The cytotoxic effects of the compounds on Jurkat T cells were evaluated using CellTox green assay (Promega). Cells (5×10^3/well) were seeded in a white-opaque 96-well plate and exposed to increasing concentrations (0.001–100 μM) of each compound or vehicle (DMSO) for 72 h. Values are means ± SE of three independent experiments and represent the concentrations causing significant (≥30%) cytotoxic effects.

4.9. Protein expression, purification and crystallization

A *N*-terminally truncated *h*DHODH (Met30-Arg396) (N10XHis-*h*DHODH30-396) [40] construct was expressed in *E. coli* BL21 (DE3) (Novagen) using a pET-19b (Novagen) expression vector containing an IPTG inducible T7-promotor. 1L of *E. coli* cultures were grown at 37 °C in terrific broth (TB) media (12 g/L tryptone, 24 g/L yeast extract, 4 g/L glycerol, 2.31 g/L KH_2PO_4, 12.54 g/L K_2HPO_4), expression was induced at OD600 0.7 with the addition of 0.2 mM IPTG and the cultures were further incubated at 16 °C for 21 h. Cells

were harvested by centrifugation at 6000g at 4 °C for 20 min 10 g of wet cells were resuspended in 40 mL of buffer A (50 mM HEPES pH 7.8, 300 mM NaCl, 10% (v/v) glycerol, 0.25% (w/v) UDAO) supplemented with 100 μL lysozyme (10 mg/mL), 10 μL DNAse (10 mg/mL) and one cOmplete EDTA free protease inhibitor tablet (Roche). All the following steps were performed at 4 °C. Pellets were homogenized with a tissue homogenizer and the cells were disrupted by two passes through an Avestin EmulsiFlex-C3 at 15000 psi. The disrupted cells were centrifuged for 1 h in 4 °C at 48500 g (Beckman Avanti J-20 centrifuge) and supernatant were collected. An ÄKTA explorer system (GE Healthcare) was used to load the cleared cell lysate at a rate of 1 mL/min onto a 5 ml HiTrap TALON crude column (GE Healthcare) pre-equilibrated with buffer A. The column was washed with buffer W (50 mM HEPES pH 7.8, 300 mM NaCl, 80 mM imidazole, 10% (v/v) glycerol and 0.25% (w/v) UDAO) until no unbound protein was eluted. A linear gradient of imidazole from 80 to 400 mM was used to elute rest of the bound protein. The fractions were checked using denaturing polyacrylamide gel electrophoresis and all *h*DHODH containing fractions were pooled and concentrated using vivaspin 20 centrifugal concentrator (Sartorius AG) with a molecular weight cut off at 30 kDa. The concentrated protein was loaded onto a Hiload Superdex 200 16/600 (GE Healthcare) column, pre-equilibrated with size exclusion buffer (100 mM HEPES pH 7.0, 400 mM NaCl, 10% (v/v) glycerol, 1 mM EDTA, 0.25% (w/v) UDAO) and eluted with a flow rate of 0.5 mL/min. The fractions corresponding to the protein peak at 442 nm were concentrated using vivaspin 20 centrifugal concentrator to a final concentration of 78 mg/mL (45 kDa, ε: 15.93 cm-1·mM-1) measured with a NanoDrop ND-1000 spectrophotometer (Saveen Werner). For crystallization, the purified protein was mixed with ORO (final concentration 2 mM) and inhibitor (final concentration 2 mM) from 50 mM stocks dissolved in DMSO and subsequently incubated at room temperature for one hour. The crystallization trials were performed using MRC 2 well sitting drop plates (Molecular Dimensions Limited) with a Mosquito robot (TTP Labtech). 300 nL protein pre-incubated with inhibitor and ORO was mixed 300 nL reservoir solution for these trials. A total of 480 sparse conditions from 5 commercially available sparse matrix screens were tested. Initial crystals appeared in several drops which were further optimized for better diffraction. Final optimized condition consisted of 0.2 M KBr, 0.2 M KSCN, 0.1 M NaAc pH 5.0, 25–35% (v/v) PEG 400, 2–5% (v/v) PGA-LM (Molecular Dimension Limited) with a 90 h preincubation at 4 °C of the protein together with 2 mM inhibitor and 2 mM ORO. As the formation of the desired cubic crystal form varied from time to time with crowding agent concentrations, a grid with concentrations varying between 25 and 35% v/v PEG 400 and 2–5% (v/v) PGA-LM was set up for each inhibitor during the crystallization. Trays were incubated at 20 °C for 7 days after which crystals were flash-cooled in liquid nitrogen.

4.10. X-ray data collection, structure determination and refinement

X-ray diffraction data were collected at 100 K on beamline ID23-2 at European Synchrotron Radiation Facility (ESRF), France using a Pilatus detector. *h*DHODH co-crystallized with compounds **4**–**6** diffracted better than 2 Å and belong to the trigonal space group $P3_221$ (Table S3). The data were indexed, integrated and scaled using the iMosflm and Scala utilities of the CCP4 program suit [41]. The crystals have one protein molecule in the asymmetric unit, corresponding to a solvent content of 68%.

The structures were determined by molecular replacement using the program Phaser [42] and the *h*DHODH (PDB id: 4YLW) as a search model. Refinement was carried out using the program Phenix [43]. Manual building was done in Coot [44]. Final structures were refined of compounds 4–6 refined to 1.85 Å, 1.95 Å and 1.75 Å, respectively. X-ray data collection and refinement statistics are summarized in Table S3.

Notes

The authors declare no competing financial interest.

PDB ID codes

The atomic coordinates and structure factors of *h*DHODH in complex with compounds **4** (PDB id: 5MVC), **5** (PDB id: 5MVD) and **6** (PDB id: 5MUT**)** have been deposited in the RCSB Protein Data Bank.

Acknowledgements

This research was financially supported by the University of Turin (*Ricerca Locale grant* 2015 (LOLMAUTO00) and 2014 (LOLM_RIC_LOC_14_01)). CHA and RCB received financial support from (LOLM_RIC_LOC_14_01) Conselho Nacional de Desenvolvimento Científico e Tecnológico (CNPq, Brazil, 481392/2013-0) and Fundação de Amparo à Pesquisa do Estado de Goiás (FAPEG, Brazil, 201210267001112 and 201310267001105). RF and MA acknowledge support from ESS & MAXIV: Cross Border network and postgraduate education programme MAX4ESSFUN. CHA is CNPq productivity fellow (310025/2015-0) and PG is long term EMBO fellow (ALTF 1163-2014). A-CM is thankful for a grant from the Equal Opportunities Commission of the Faculty of Chemistry of Bielefeld University. RCB and CHA would like to thank ChemAxon for providing the academic license of their software, as well as Brazilian funding agencies CNPq, CAPES and FAPEG.

Authors wish to thank several persons who gave their contributions, for the final results. In particular, we would like to mention Dr. Annalisa Costale, for performing all the UHPLC analysis. Dr. Livio Stevanato for performing all the NMR experiments and for maintenance of the instrument, Prof. Alessandro Barge for performing HPLC related support and in general for useful discussions and Dr. Renzo Bagnati (Istituto di Ricerce Farmacologiche Mario Negri, Milano (IT)) for support on HRMS experiments. We want also thank Dr. Davide Bonanni for supporting the manuscript in the production of the crystallographic images.

We thank the European Synchrotron Radiation Facility (ESRF) for beam time allocation and access.

Appendix A. Supplementary data

Supplementary data related to this article can be found at http://dx.doi.org/10.1016/j.ejmech.2017.02.017.

References

[1] V.K. Vyas, B. Variya, M.D. Ghate, Design, synthesis and pharmacological evaluation of novel substituted quinoline-2-carboxamide derivatives as human dihydroorotate dehydrogenase (hDHODH) inhibitors and anticancer agents, Eur. J. Med. Chem. 82 (2014) 385–393.

[2] J. Leban, D. Vitt, Human dihydroorotate dehydrogenase inhibitors, a novel approach for the treatment of autoimmune and inflammatory diseases, Arzneim. Forsch. 61 (2011) 66–72.

[3] A. Singh, M. Maqbool, M. Mobashir, N. Hoda, Dihydroorotate dehydrogenase: a drug target for the development of antimalarials, Eur. J. Med. Chem. 125 (2017) 640–651.

[4] M.L. Herrmann, R. Schleyerbach, B.J. Kirschbaum, Leflunomide: an immunomodulatory drug for the treatment of rheumatoid arthritis and other autoimmune diseases, Immunopharmacology 47 (2000) 273–289.

[5] M.L. Lolli, M. Giorgis, P. Tosco, A. Foti, R. Fruttero, A. Gasco, New inhibitors of dihydroorotate dehydrogenase (DHODH) based on the 4-hydroxy-1,2,5-oxadiazol-3-yl (hydroxyfurazanyl) scaffold, Eur. J. Med. Chem. 49 (2012) 102–109.

[6] H. Munier-Lehmann, P.-O. Vidalain, F. Tangy, Y.L. Janin, On dihydroorotate

dehydrogenases and their inhibitors and uses, J. Med. Chem. 56 (2013) 3148–3167.
[7] W. Knecht, M. Löffler, Species-related inhibition of human and rat dihydroorotate dehydrogenase by immunosuppressive isoxazol and cinchoninic acid derivatives, Biochem. Pharmacol. 56 (1998) 1259–1264.
[8] R.I. Fox, M.L. Herrmann, C.G. Frangou, G.M. Wahl, R.E. Morris, V. Strand, B.J. Kirschbaum, Mechanism of action for leflunomide in rheumatoid arthritis, Clin. Immunol. 93 (1999) 198–208.
[9] G.J. Peters, S.L. Sharma, E. Laurensse, H.M. Pinedo, Inhibition of pyrimidine de novo synthesis by DUP-785 (NSC 368390), Invest.. New Drugs 5 (1987) 235–244.
[10] O.P. Kulkarni, S.G. Sayyed, C. Kantner, M. Ryu, M. Schnurr, M. Sardy, J. Leban, R. Jankowsky, A. Ammendola, R. Doblhofer, H.-J. Anders, 4SC-101, a novel small molecule dihydroorotate dehydrogenase inhibitor, suppresses systemic lupus erythematosus in MRL-(Fas)lpr mice, Am. J. Pathol. 176 (2010) 2840–2847.
[11] 4SC, 4SC pipeline, in.
[12] S. Li, G. Luan, X. Ren, W. Song, L. Xu, M. Xu, J. Zhu, D. Dong, Y. Diao, X. Liu, L. Zhu, R. Wang, Z. Zhao, Y. Xu, H. Li, Rational design of benzylidenehydrazinyl-substituted thiazole derivatives as potent inhibitors of human dihydroorotate dehydrogenase with in vivo anti-arthritic activity, Sci. Rep. 5 (2015) 14836.
[13] H. Munier-Lehmann, M. Lucas-Hourani, S. Guillou, O. Helynck, G. Zanghi, A. Noel, F. Tangy, P.-O. Vidalain, Y.L. Janin, Original 2-(3-Alkoxy-1H-pyrazol-1-yl)pyrimidine derivatives as inhibitors of human dihydroorotate dehydrogenase (DHODH), J. Med. Chem. 58 (2015) 860–877.
[14] J. Zhu, L. Han, Y. Diao, X. Ren, M. Xu, L. Xu, S. Li, Q. Li, D. Dong, J. Huang, X. Liu, Z. Zhao, R. Wang, L. Zhu, Y. Xu, X. Qian, H. Li, Design, synthesis, x-ray crystallographic analysis, and biological evaluation of thiazole derivatives as potent and selective inhibitors of human dihydroorotate dehydrogenase, J. Med. Chem. 58 (2015) 1123–1139.
[15] M. Lucas-Hourani, H. Munier-Lehmann, F. El Mazouni, N.A. Malmquist, J. Harpon, E.P. Coutant, S. Guillou, O. Helynck, A. Noel, A. Scherf, M.A. Phillips, F. Tangy, P.-O. Vidalain, Y.L. Janin, Original 2-(3-Alkoxy-1H-pyrazol-1-yl) azines inhibitors of human dihydroorotate dehydrogenase (DHODH), J. Med. Chem. 58 (2015) 5579–5598.
[16] R. Baumgartner, M. Walloschek, M. Kralik, A. Gotschlich, S. Tasler, J. Mies, J. Leban, Dual binding mode of a novel series of DHODH inhibitors, J. Med. Chem. 49 (2006) 1239–1247.
[17] S. Bonomo, P. Tosco, M. Giorgis, M. Lolli, R. Fruttero, The role of fluorine in stabilizing the bioactive conformation of dihydroorotate dehydrogenase inhibitors, J. Mol. Model. 19 (2013) 1099–1107.
[18] A.C. Pippione, F. Dosio, A. Ducime, A. Federico, K. Martina, S. Sainas, B. Froelund, M. Gooyit, K.D. Janda, D. Boschi, M.L. Lolli, Substituted 4-hydroxy-1,2,3-triazoles: synthesis, characterization and first drug design applications through bioisosteric modulation and scaffold hopping approaches, MedChemComm 6 (2015) 1285–1292.
[19] S. Liu, E.A. Neidhardt, T.H. Grossman, T. Ocain, J. Clardy, Structures of human dihydroorotate dehydrogenase in complex with antiproliferative agents, Structure (London, U. K.) 8 (2000) 25–33.
[20] J. Leban, M. Kralik, J. Mies, R. Baumgartner, M. Gassen, S. Tasler, Biphenyl-4-ylcarbamoyl thiophenecarboxylic acids as potent DHODH inhibitors, Bioorg, Med. Chem. Lett. 16 (2006) 267–270.
[21] VS The PyMOL Molecular Graphics System, LLC., Version 1.8 Schrödinger, LLC.
[22] L.M. Weinstock, P. Davis, B. Handelsman, R.J. Tull, General synthetic system for 1,2,5-thiadiazoles, J. Org. Chem. 32 (1967) 2823–2828.
[23] A.B. Sheremetev, Y.A. Strelenko, T.y.S. Novikova, L.I. Khmel'nitskii, 1,2,5-oxadiazoles substituted at ring nitrogen. part 1. synthesis and study of 2-ethyl-1,2,5-oxadiazol-3(2H)-ones, Tetrahedron 49 (1993) 5905–5914.
[24] K. Masuda, J. Adachi, K. Nomura, Studies on mesoionic compounds. Part 10. Synthesis and chemical properties of mesoionic 1,2,5-thiadiazolium-3-olates, J. Chem. Soc. Perkin Trans. 1 (1981) 1033–1036.
[25] S. Sainas, Bioisosteric modulation of salicylamide in the design of Plasmodium falciparum dihydroorotate dehydrogenase (PfDHODH) inhibitors. Master Thesis, in: Dipartimento di Scienza e Tecnologia del Farmaco, Turin University, Turin, 2013.
[26] A. Ducime, New bioisosteric applications of hydroxylated azoles in drug design, PhD thesis, in: Dipartimento di Scienza e Tecnologia del Farmaco, Turin University, Turin, 2016.
[27] T.T. Talele, The "cyclopropyl fragment" is a versatile player that frequently appears in preclinical/clinical drug molecules, J. Med. Chem. 59 (2016) 8712–8756.
[28] C. Wang, Y. Han, A. Wu, S. Solyom, L. Niu, Mechanism and site of inhibition of AMPA receptors: pairing a thiadiazole with a 2,3-benzodiazepine scaffold, ACS Chem. Neurosci. 5 (2014) 138–147.
[29] B.R. Beno, K.-S. Yeung, M.D. Bartberger, L.D. Pennington, N.A. Meanwell, A survey of the role of noncovalent sulfur interactions in drug design, J. Med. Chem. 58 (2015) 4383–4438.
[30] H.M. Cherwinski, R.G. Cohn, P. Cheung, D.J. Webster, Y.Z. Xu, J.P. Caulfield, J.M. Young, G. Nakano, J.T. Ransom, The immunosuppressant leflunomide inhibits lymphocyte proliferation by inhibiting pyrimidine biosynthesis, J. Pharmacol. Exp. Ther. 275 (1995) 1043–1049.
[31] K. Rückemann, L.D. Fairbanks, E.A. Carrey, C.M. Hawrylowicz, D.F. Richards, B. Kirschbaum, H.A. Simmonds, Leflunomide Inhibits Pyrimidine de Novo Synthesis in Mitogen-stimulated T-lymphocytes from Healthy Humans, J. Biol. Chem. 273 (1998) 21682–21691.
[32] T.L. Forrest, R.E. Ware, T. Howard, B.D. Jaffee, S.M. Denning, Novel mechanisms of brequinar sodium immunosuppression on T cell activation, Transplantation 58 (1994) 920–926.
[33] M.C. Kraan, T.J. Smeets, M.J. van Loon, F.C. Breedveld, B.A. Dijkmans, P.P. Tak, Differential effects of leflunomide and methotrexate on cytokine production in rheumatoid arthritis, Ann. Rheum. Dis. 63 (2004) 1056–1061.
[34] L. Li, J. Liu, T. Delohery, D. Zhang, C. Arendt, C. Jones, The effects of teriflunomide on lymphocyte subpopulations in human peripheral blood mononuclear cells in vitro, J. Neuroimmunol. 265 (2013) 82–90.
[35] B. Aungst, J. Blake, N. Rogers, B. Dusak, Effects of plasma protein binding displacement on the pharmacokinetics, tissue and tumor concentrations and efficacy of brequinar, a highly protein-bound antitumor agent, J. Pharmacol. Exp. Ther. 253 (1990) 230.
[36] B. Jursic, N. Bregant, The selective methylation of 4-(ethoxycarbonyl)-3-methylpyrazolin-5-one with dimethyl sulfate, Synth. Commun. 19 (1989) 2087–2093.
[37] A.E. Cho, V. Guallar, B.J. Berne, R. Friesner, Importance of accurate charges in molecular docking: quantum mechanical/molecular mechanical (QM/MM) approach, J. Comput. Chem. 26 (2005) 915–931.
[38] M. Giorgis, M.L. Lolli, B. Rolando, A. Rao, P. Tosco, S. Chaurasia, D. Marabello, R. Fruttero, A. Gasco, 1,2,5-Oxadiazole analogues of leflunomide and related compounds, Eur. J. Med. Chem. 46 (2011) 383–392.
[39] J. Rao, W.R. Otto, Fluorimetric DNA assay for cell growth estimation, Anal. Biochem. 207 (1992) 186–192.
[40] B. Walse, V.T. Dufe, B. Svensson, I. Fritzson, L. Dahlberg, A. Khairoullina, U. Wellmar, S. Al-Karadaghi, The structures of human dihydroorotate dehydrogenase with and without inhibitor reveal conformational flexibility in the inhibitor and substrate binding sites, Biochemistry 47 (2008) 8929–8936.
[41] The CCP4 suite, Programs for protein crystallography, acta crystallographica section D, Biol. Crystallogr. 50 (1994) 760–763.
[42] A.J. McCoy, R.W. Grosse-Kunstleve, P.D. Adams, M.D. Winn, L.C. Storoni, R.J. Read, Phaser crystallographic software, J. Appl. Crystallogr. 40 (2007) 658–674.
[43] P.D. Adams, P.V. Afonine, G. Bunkóczi, V.B. Chen, I.W. Davis, N. Echols, J.J. Headd, L.W. Hung, G.J. Kapral, R.W. Grosse-Kunstleve, A.J. McCoy, N.W. Moriarty, R. Oeffner, R.J. Read, D.C. Richardson, J.S. Richardson, T.C. Terwilliger, P.H. Zwart, PHENIX: a comprehensive Python-based system for macromolecular structure solution, Acta Crystallographica Section D, Biol. Crystallogr. 66 (2010) 213–221.
[44] P. Emsley, B. Lohkamp, W.G. Scott, K. Cowtan, Features and development of Coot, acta crystallographica section D, Biol. Crystallogr. 66 (2010) 486–501.